



## THEORY OF MULTIPLE BUBBLE GROWTH IN POROUS MEDIA BY SOLUTE DIFFUSION

X. LI and Y. C. YORTSOS\*

Petroleum Engineering Program, Department of Chemical Engineering, University of Southern California, Los Angeles, CA 90089-1211, U.S.A.

(First received 18 October 1993; accepted in revised form 7 March 1994)

**Abstract**—We present a theoretical analysis of bubble growth in porous media by solute diffusion. Based on visualization experiments, a theoretical model is developed for bubble growth driven by a constant or a time-varying supersaturation in the far-field. It is shown that in porous media, gas evolution (patterns and rates) is much different than in the bulk. Patterns and rates of growth are identified for single and multiple gas clusters, using statistical models, such as percolation and diffusion-limited-aggregation (DLA). The effect of (heterogeneous) nucleation on the growth of multiple clusters is analyzed. Particular emphasis is placed on the critical gas saturation,  $S_{gc}$ , which denotes the critical value of the pore volume fraction occupied by the gas for the formation of a sample-spanning cluster. This quantity is studied in terms of the system parameters, notably the nucleation fraction and the pressure decline rate (pressure/time).  $S_{gc}$  is found to increase with the nucleation fraction and the pressure decline rate at relatively high rates, but to be independent of the latter at sufficiently small rates. The scaling of these results is also discussed.

## 1. INTRODUCTION

The evolution of gas saturation (bubble growth) in porous media is important to applications, such as solution gas-drive (Hunt and Berry, 1956; Firoozabadi *et al.*, 1989; Kortekaas and Poelgeest, 1989; Moulu and Longeron, 1989; Kamath and Boyer, 1993), which is a common method for the recovery of oil from underground reservoirs, and boiling processes. Boiling in porous media is encountered in diverse fields, including geothermal reservoirs (Schubert and Straus, 1977), nuclear waste disposal (Doughty and Pruess, 1988) and enhanced heat transfer (Thome, 1990). Although the concepts presented are also applicable to boiling we shall focus in this paper on the first problem only, where the growth of the gas phase is driven by mass transfer. Contrary to *external* displacements in porous media, where a fluid phase displaces another immiscible phase at a specified injection rate, which are well understood, *internal* displacements by an *in situ* growing phase, driven by diffusion, are still subject to controversy and confusion. This is true both for evaporation and condensation processes. The basic reason is the complex interplay of a multitude of factors, such as nucleation, diffusion, capillarity and viscous forces, all of which contribute to the growth of gas clusters (bubbles) in porous media, but which have not yet been treated in a comprehensive manner. In the majority of previous studies (Hunt and Berry, 1956; Moulu and Longeron, 1989; Kashchiev and Firoozabadi, 1993a b), bubble growth in porous media has been approached follow-

ing models for growth in the bulk (Scriven, 1959; Szekely and Martins, 1971; Szekely and Fang, 1973; Plesset and Prosperetti, 1977), which is a questionable approach, given the disordered structure of the gas phase in a real porous medium.

To address porous media effects, we have recently investigated the application of percolation concepts (Yortsos and Parlari, 1989) and also proceeded with a visualization study (Li and Yortsos, 1991). Yortsos and Parlari (1989) studied certain aspects of nucleation and bubble growth and derived a percolation model valid at conditions of very low pressure decline rates. Their emphasis was on the concept of the *critical gas saturation*,  $S_{gc}$ , which denotes the onset of free gas flow and was defined by the authors as the value that signals the formation of a sample-spanning gas cluster. As is conventional in the porous media literature, by saturation of a fluid we denote the fraction of the pore volume occupied by that phase. Yortsos and Parlari (1989) found that the nucleation fraction and the geometric and topological features of the porous medium significantly affect  $S_{gc}$ . Li and Yortsos (1991) presented visualization studies similar to Danesh *et al.* (1987) and Yousfi *et al.* (1990) that showed the existence of disordered patterns in model porous media (Fig. 1), and proceeded to develop a simplified pore network simulator. The simulator matched quite well the visualization experiments. Despite these efforts, however, a theory for bubble growth in porous media is currently lacking. It is the purpose of this paper to provide a systematic study in this direction.

We analyze single and multiple bubble growth with emphasis on the multiple bubble problem. Specifically, we examine growth patterns and rates of growth and the effects of the process parameters. In two

\*Author to whom correspondence should be addressed.

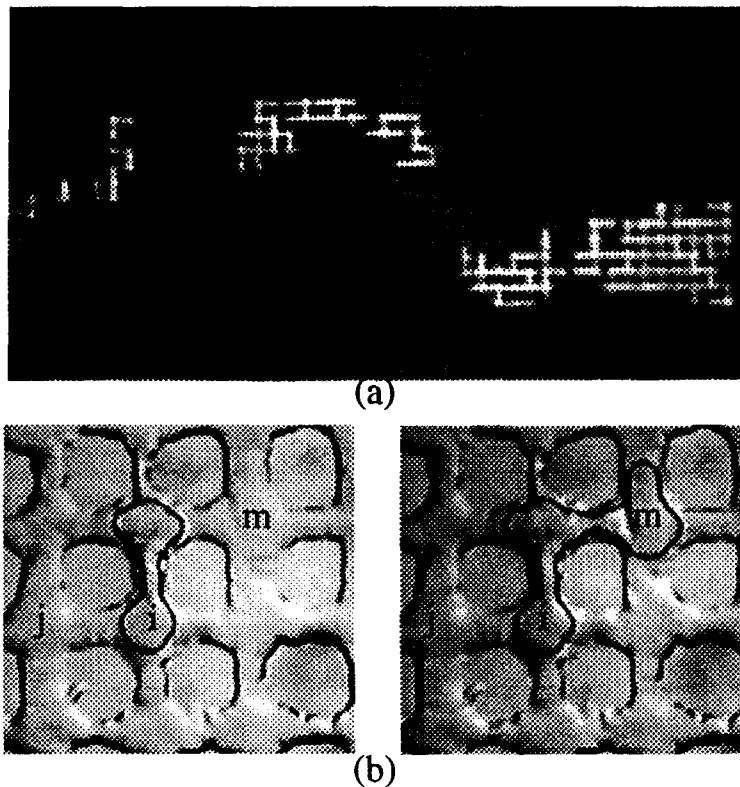


Fig. 1. Snapshots of gas cluster growth from carbonated water in a glass micromodel: (a) large scale view; (b) pore level sequence.

companion papers (Li and Yortsos, 1994; Satik *et al.*, 1995), we have discussed aspects of *single* bubble growth. Li and Yortsos (1994) considered the interface stability for a single bubble in *effective* porous media (such as a Hele–Shaw cell). Satik *et al.* (1995) reported on the scaling behavior of single bubble growth in random media, where the scaling laws were found to be different from the classical. Here, we consider the general multiple growth problem in random porous media. Although the scope of the paper is general, a more specific objective is to determine  $S_{gc}$  which is an important variable in applications. This quantity reflects the cumulative effect of various processes, such as nucleation, cluster growth and competition and the effect of the rate of change of supersaturation. From a practical viewpoint,  $S_{gc}$  signals the onset of bulk gas flow, which is usually undesirable in the recovery of the liquid oil phase, and it is a key parameter in commercial simulators.

Several laboratory studies have been conducted on  $S_{gc}$  before. Research has focused on determining its value and its dependence on various parameters, notably the pressure decline rate (pressure/time). Different values of  $S_{gc}$  were reported by different authors. Handy (1958) relied on gas expansion during flow in laboratory experiments to report critical gas saturations in the range 4–11%. Moulu and Longeron (1989) estimated  $S_{gc}$  values from 6% for field conditions to 12% for laboratory conditions. In the experi-

ments of Firoozabadi *et al.* (1989), values less than 0.5% were reported. Kortekaas and Poelgeest (1989) measured  $S_{gc}$  values which varied from 7 to 27%. Platt and Lewis (1969) using field data estimated a critical gas saturation value of 27%. Finally, some investigators have suggested that  $S_{gc}$  is the same with the breakthrough gas saturation in an external displacement [where gas displaces an immiscible oil, Chowdiah (1987)]. In the latter case,  $S_{gc}$  ought to be infinitesimally small.

The effect of the pressure decline rate  $a$  has also been studied (Hunt and Berry, 1956; Firoozabadi *et al.*, 1989; Kortekaas and Poelgeest, 1989; Moulu and Longeron, 1989; Kamath and Boyer, 1993). This quantity denotes the time rate of change of the far-field pressure, and also measures the change in the degree of supersaturation. The general consensus is that  $S_{gc}$  increases with an increase in  $a$ , presumably as a result of an increase in the nucleation fraction, and some of the experiments have indeed shown such trends. Implicit to this argument is the assumption of a reproducibility of nucleation events as  $a$  varies, which can be consistent only when nucleation is based on specific nucleation sites. This type of heterogeneous nucleation was proposed by Yortsos and Parlar (1989) [see also Crum (1982); Atchley and Prosperetti (1989)]. At the same time, experiments in low permeability rocks, where capillarity is strong, have shown negligible effects of  $a$ , at least in the range

investigated [order of psi/day, Kamath and Boyer (1993)]. These latter findings are consistent with the low pressure decline rate model of Yortsos and Parlal (1989), where capillarity dominates cluster growth. Interesting aspects of gas displacement in external drives in the presence of gravity were reported by Dumoré (1970).

From the above, it is apparent that  $S_{gc}$  depends on a multitude of factors, such as the extent of nucleation, the competition between growing clusters and the rate of decline of the supersaturation. For its determination, therefore, the general multiple cluster growth problem must be analyzed. It should be noted, however, that sometimes the estimation of  $S_{gc}$  has been obscured with problems in data interpretation. For example, the practice is often taken to estimate  $S_{gc}$  as the gas saturation when gas first appears at the medium outlet. This can be misleading. Because of the possibility of nucleation sites and the subsequent cluster growth in the vicinity of the outlet, such evidence of macroscopic flow is unrelated to the formation of a sample-spanning gas cluster (see, for example, Fig. 1). In fact, in the former case, the reported saturation would be a stochastic variable characterized by a probability distribution and the interpretation of results should be done carefully. For example, in a particular experimental realization, Li and Yortsos (1991) found that such a value of  $S_{gc}$  decreased as the pressure decline rate increased. A robust definition of  $S_{gc}$  should involve the formation of a sample-spanning cluster. This definition was introduced for the first time by Yortsos and Parlal (1989), it is consistent with the experiments of Kortekaas and Poelgeest (1989) and will be used in the remainder of this work.

The paper is organized as follows: Section 2 describes the theoretical formulation of the problem. We briefly discuss the mode of nucleation and the steps involved in bubble growth in porous media based on observations from visualization experiments (Li and Yortsos, 1991). Depending on the particular mode of supersaturation applied, three cases of bubble growth will be considered (see below). A common dimensionless description for all three cases is derived. Section 3 discusses the growth of a single cluster. Although a summary of part of this problem can also be found in Satik *et al.* (1995), the description of single bubble growth is necessary before the main topic of multiple bubble growth is analyzed. Subsequently, we consider the general problem of growth of multiple gas clusters (Section 4). Patterns and rates of growth are derived for various conditions. Depending on the magnitude of the capillary forces, the nucleation characteristics, the depletion of supersaturation and the mass transfer mode, three specific regimes are identified. Finally, Section 5 addresses the determination of  $S_{gc}$  and the effects of various parameters, such as the nucleation fraction and the pressure decline rate. Throughout the text, it is necessary to make references to related papers in various stages of publication (Yortsos and Parlal, 1989; Li and Yortsos, 1991, 1994; Satik *et al.*, 1995).

## 2. THEORETICAL FORMULATION

Bubble growth in porous media is typically driven by the application of one of the following conditions:

- (i) Fixed supersaturation, where the pressure of the liquid in the far-field or in the production outlet is suddenly lowered (or raised) to a constant value, which remains constant for the remainder of the process.
- (ii) Constant liquid withdrawal from one or multiple outlets, at a fixed volumetric flow rate.
- (iii) Constant rate of increase of supersaturation, where the liquid pressure in the far-field or in the production outlet is reduced at a fixed rate,  $a$ .

All these three cases will be considered here. The liquid-to-gas phase change occurs by two consecutive processes, nucleation and bubble growth. Nucleation in the present context was discussed in Yortsos and Parlal (1989). Because of the relevance to the multiple growth problem, it is also briefly discussed below, before the general problem of growth by solute diffusion is analyzed. As is conventional in porous media studies (Dullien, 1992), the porous medium is represented by an equivalent network of nodes (pores or pore bodies) and bonds (pore throats) of distributed sizes. Figure 1 is a characteristic representation of the assumed structure. Further details are discussed later.

### 2.1. Nucleation

Multiple clusters arise from nucleation at different nucleation sites, and occur at various stages depending on the particular process (Kennedy and Olson, 1952; Stewart *et al.*, 1953; Wieland and Kennedy, 1957; Chatenever *et al.*, 1959; Hoyos *et al.*, 1990). By nucleation we refer here to the onset of the appearance of a *macroscopic* bubble (defined as that which would occupy a pore body or its fraction). In a previous publication (Yortsos and Parlal, 1989), we examined various nucleation mechanisms and concluded that *heterogeneous* nucleation is the most plausible mechanism in porous media. Such bubbles arise from various sites on the pore walls containing trapped gas (either pre-existent or nucleated), which is released (the sites become activated), when the local supersaturation exceeds the capillary pressure of the site. For example, for a site in the form of a conical cavity of mouth radius  $W$  (Fig. 2), the activation condition would be

$$KC - P_l \geq \frac{2\gamma}{W} \quad (1)$$

where concentration and liquid pressure are evaluated at the interface,  $\gamma$  is the interfacial tension and linear phase equilibria were assumed. More generally, condition (1) applies to sites of various geometries, provided that  $W$  denotes an appropriate length (usually the smallest constriction in a converging-diverging geometry). Activation of sites in this fashion was reviewed extensively by Atchley and Prosperetti

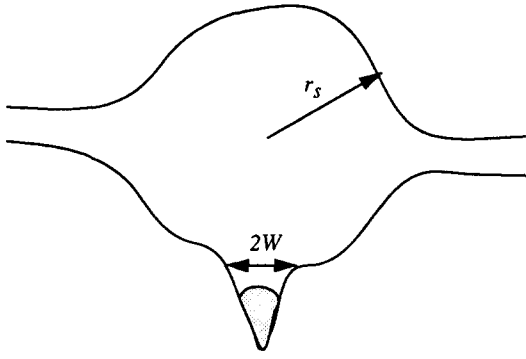


Fig. 2. Schematic of a nucleation site of radius  $W$  in a pore body or radius  $r_s$  (cavity size is exaggerated).

(1989) and by Crum (1982). Analogous conclusions were also reached by Yousfi *et al.* (1991). In this model, therefore, the nucleation condition depends only on the local variables  $C$  and  $P_i$ , and does not involve the intrinsic kinetics of classical nucleation (whether homogeneous or heterogeneous). This important distinction was not made in earlier publications on solution gas-drive, where classical kinetics were used. However, typical experiments in porous media rarely reach the very large degrees of supersaturation required for homogeneous nucleation [see also Kamath and Boyer (1993)].

In another approach, it was recently suggested that nucleation in porous media occurs "instantaneously", namely in multiple sites at the same instant (Kashchiev and Firoozabadi, 1993). This notion probably derives from homogeneous nucleation theory, which in the complete absence of surface heterogeneities, predicts the simultaneous formation of a multitude of nuclei. However, "instantaneous" nucleation is also possible in our context, although only in the special case of a sudden step increase in supersaturation, which is sufficiently large for a number of nucleation sites to be simultaneously activated (see below). In the general case, where the change in supersaturation is gradual, as in (iii) above, an instantaneous nucleation mechanism is doubtful. Instead, it is the pressure decline rate and the distribution of sites, which determine the ensuing activation of sites and bubble growth and affect the apparent "nucleation" rates and the critical gas saturation.

## 2.2. Bubble growth

Following nucleation, we consider, next, the mathematical formulation of bubble growth for the case of the solution gas-drive problem. Similar considerations apply for the boiling problem but will not be presented here. We assume a two-component liquid, one component of which is volatile. Without loss in generality, we consider approximate phase equilibria. In the gas cluster denoted by subscript  $k$ , the ideal gas law applies

$$P_{gk} V_k = n_k \mathcal{R} T \quad (2)$$

where  $P_{gk}$  is the gas pressure,  $V_k$  the cluster volume,  $n_k$  its mole content,  $\mathcal{R}$  the ideal gas constant and  $T$  the temperature. Gas-liquid interfaces are located at pore throats in the cluster perimeter [Fig. 1(b)]. We assume thermodynamic equilibrium and linear phase equilibria

$$P_{gk} = K C_k \quad (3)$$

where  $C_k$  is the solute concentration at the cluster interface and  $K$  the solubility constant. Growth occurs by mass transfer over the cluster interface area,  $A_k$ ,

$$M_w \frac{dn_k}{dt} = \int_{A_k} D \frac{\partial C}{\partial n} dA \quad (4)$$

where  $M_w$  is the molecular weight of the solute and  $\mathbf{n}$  is the outwards pointing normal. The solute transport obeys a convection-diffusion equation with diffusion coefficient  $D$ , which in a continuum formalism reads

$$\phi \frac{\partial C}{\partial t} + \mathbf{u} \cdot \nabla C = \phi D \nabla^2 C \quad (5)$$

where  $\phi$  is porosity. The velocity field is given by Darcy's law

$$\mathbf{u} = -\frac{k}{\mu} \nabla P \quad (6)$$

$$\nabla \cdot \mathbf{u} = 0 \quad (7)$$

where gravity effects were neglected (see also below). For simplicity, we may absorb  $\phi$  into  $t$  and  $D$ , and proceed by considering the mass balance (5) with  $\phi = 1$ . These balances are appropriately recast in terms of finite differences to describe the problem in a disordered pore network (Li and Yortsos, 1991).

Contrary to the bulk, gas clusters in porous media are not spherical but disordered, although menisci have a spherical geometry locally. Figure 1 from the glass micromodel experiments of Li and Yortsos (1991), who studied the growth of  $\text{CO}_2$  gas from saturated carbonated water, gives a clear demonstration of these features. In particular, *fractal* structures, as a result of a percolation or viscous fingering process, are quite likely. The menisci in the cluster perimeter may be stationary or moving. A meniscus is locked in place and cannot invade an adjacent pore throat when its capillary pressure threshold is not met

$$P_{gk} - P_{lj} \leq \frac{2\gamma}{r_{ij}} \quad (8)$$

where  $r_{ij}$  is the pore throat radius connecting a gas-occupied pore  $i$  to an adjacent liquid-occupied pore  $j$  and  $P_{lj}$  is the liquid pressure at pore  $j$  [Fig. 1(b)]. When the capillary pressure is sufficiently high for the threshold to be exceeded, however, the meniscus can advance through the pore throat to fill the particular pore [e.g. pore  $m$  in Fig. 1(b)], much like in a drainage process. Although the process of growth of a gas cluster is generally complex, it can be simplified by identifying two key steps observed experimentally:

A *pressurization* step, during which all interfaces in the cluster are locked (or only slightly advancing) and the gas pressure steadily increases

$$V_k \frac{dP_{gk}}{dt} = \mathcal{R}T \frac{dn_k}{dt} \quad (9)$$

until the first capillary threshold at the perimeter is reached.

A *pore-filling* step, immediately following the pressurization step, during which one or more perimeter throats have been penetrated, gas partially occupies the newly invaded pores, and both pressure and volume (but mostly volume) change according to

$$P_{gk} \frac{dV_k}{dt} + \left( V_k \frac{dP_{gk}}{dt} \right) = \mathcal{R}T \frac{dn_k}{dt} \quad (10)$$

where the term in parentheses accounts for possible expansion. During this step, we assume that the capillary pressure in the invaded pore is negligible. In either step, the rate of mass transfer to the gas cluster is given by eq. (4) above. In general, several menisci may be advancing at the same time, while others may be locked because of capillarity. Various additional remarks on these two steps are given in Appendix A.

In all applications (i)–(iii), we use the same initial condition

$$C = C_0, \quad P_l = P_0 = KC_0 \quad \text{at } t = 0 \quad (11)$$

but different boundary conditions, depending on the particular process. For case (i), we take

$$C = C_0, \quad P_l = P_\infty < P_0 \quad \text{at } |\mathbf{x}| \rightarrow \infty \quad (12)$$

or, for a finite system,

$$\frac{\partial C}{\partial n} = 0 \quad \text{at the system boundaries.} \quad (13)$$

The latter applies both to impervious and to flow boundaries (where it becomes equivalent to Dankwerts' condition). The other boundary conditions are

$$- \int_{S_p} \frac{k}{\mu} \frac{\partial P}{\partial n} dS = Q \quad (14)$$

where  $S_p$  is the production area, for case (ii), and

$$P_l = P_0 - at \quad \text{at } |\mathbf{x}| \rightarrow \infty \quad \text{or at the production ports} \quad (15)$$

for case (iii), where  $a$  is the pressure decline rate.

### 2.3. Dimensionless formulation

It is useful to introduce a common dimensionless notation, with dimensionless variables denoted by subscript  $D$ . First, we define the applied supersaturation,  $S = (P_0 - P_\infty)/P_0$ . It is constant for case (i), where it is also known as the *Jakob* number

$$Ja = \frac{P_0 - P_\infty}{P_0} = \frac{C_0 - C_\infty}{C_0} \quad (16)$$

but it is generally variable, in a manner to be deter-

mined, for case (ii), and increasing with time,  $S = at/P_0$ , for case (iii). We scale velocity based on the diffusive driving force, by taking its characteristic value  $u^*$  to be  $DJa/l^*$ ,  $Q/l^{*2}$  and  $\sqrt{Da/P_0}$ , in the three cases, respectively, where we also introduced the characteristic length  $l^*$ . The latter scales diffusion, and may be different for different applications, as discussed below. The characteristic time  $t^*$  is taken to be  $t^* = l^*/u^*$ .

Next, a dimensionless pressure is defined,  $P_D = (P - P_\infty)/(P_0 - P_\infty)\Pi_1$ , where  $P_\infty$  refers to far-field pressure [which is fixed for case (i), but varies with time for the other two cases, in an unspecified manner for case (ii), and linearly in time,  $P_\infty = P_0 - at$ , for case (iii)]. With this definition, the far-field condition is  $P_D = 0$  (or no-flux) in all cases. The dimensionless number  $\Pi_1 \equiv D\mu/kP_0$  measures the pressure drop in the liquid due to flow induced by diffusion. It is typically small (of the order of  $10^{-3}$  for  $k = 1$  md,  $P_0 = 1000$  psi,  $D = 10^{-5}$  cm<sup>2</sup>/s, and  $\mu = 1$  cp). In this notation, the momentum balance reads

$$\mathbf{u}_D = -\nabla P_D \quad (17)$$

$$\mathbf{u}_D = -\lambda_D \nabla P_D \quad (18)$$

$$\mathbf{u}_D = -t_D \nabla P_D \quad (19)$$

for the three cases, where we defined the time-dependent variable  $\lambda_D = Sl^*D/Q$  for case (ii). For convenience, we can introduce the further substitution  $\mathbf{u}_D = \mathbf{v}_D$ ,  $\mathbf{u}_D = \mathbf{v}_D \lambda_D$  and  $\mathbf{u}_D = \mathbf{v}_D t_D$  in the respective three cases, to reduce eqs (17)–(19) to a common notation.

Next, we define a dimensionless concentration  $C_D$ , such that it takes the value one in the far-field, and a value near zero at the cluster interface. The appropriate definition for all cases is

$$C_D = 1 + \frac{C - C_0}{C_0 S}. \quad (20)$$

It is also convenient to introduce new time scales. We shall define  $d\tau = dt_D$ ,  $d\tau = \lambda_D dt_D$ , and  $d\tau = t_D dt_D$  for the respective three cases, which can also be commonly expressed as  $d\tau = (SD/l^{*2})dt_D$ . The latter illustrates that the appropriate time scaling in all processes is diffusion-based. In this notation, the mass balance on the solute becomes

$$S \left[ \frac{\partial C_D}{\partial \tau} + \mathbf{v}_D \cdot \nabla C_D + (C_D - 1) \frac{d \ln S}{d\tau} \right] = \nabla^2 C_D \quad (21)$$

for all cases subject to the conditions  $C_D = 1$  at  $\tau = 0$  and in the far-field and to a no-flux condition at the interface boundaries. The important *quasi-static* limit  $\nabla^2 C_D = 0$  is obtained at weak supersaturations,  $S \ll 1$  (see also below). It is important to note that the latter condition is time-dependent for cases (ii) and (iii).

Finally, we proceed to cast the interface conditions in dimensionless form. Condition (3) reduces to

$$\Pi_1 P_{Dg} = C_{Dk} \quad (22)$$

which, in view of  $\Pi_1 \ll 1$ , also implies  $C_{Dk} \ll 1$ . This result derives from the negligible pressure drop in the liquid under typical bubble growth conditions and will be repeatedly used below. Nonetheless, the coupling between pressure and concentration cannot be neglected.

The condition for the penetration of a perimeter bond, inequality (8), is now expressed as

$$P_{Dg} - P_{Dij} \leq \frac{2}{Ca} \frac{1}{r_{Dij}} \quad (23)$$

where we introduced the capillary number,

$$Ca = \frac{D\mu r^*}{\gamma k} S \quad (24)$$

and  $r^*$  is a characteristic pore size. Clearly,  $Ca$  is the product of two factors, one based on the diffusion velocity  $D\mu r^*/\gamma k$  and another based on the applied supersaturation. Again, for cases (ii) and (iii),  $Ca$  is time-varying. Finally, dimensionless growth and pressurization conditions can be obtained. The pressurizing step condition (9) reads as follows:

$$V_{Dk} \frac{d}{d\tau} [\Pi_1 S P_{Dgk} + 1 - S] = \alpha \int_{ADk} \frac{\partial C_D}{\partial n_D} dA_D \quad (25)$$

where the dimensionless solubility constant  $\alpha = \mathcal{R}T/M_w K$  was defined, while the filling step (10) is described by

$$(SC_{Dk} + 1 - S) \frac{dV_{Dk}}{d\tau} = \alpha \int_{ADk} \frac{\partial C_D}{\partial n_D} dA_D \quad (26)$$

assuming negligible expansion. We conclude that the important dimensionless variables that emerge from the above are the level of supersaturation  $S$ , the capillary number  $Ca$  and the two parameters  $\alpha$  and  $\Pi_1$ .

The solution of the problem of bubble growth in porous media is best obtained with a pore network simulator. Pore network simulations are useful for understanding displacements in porous media and have been frequently used. Here, the porous medium is represented by an equivalent network of pores of distributed sizes, joined by bonds of a different size distribution. Pores are taken to represent the storage capacity, bonds represent flow resistance and provide capillary pressure thresholds. For immiscible displacement, interfaces are allowed to reside in pore bodies only, the occupancy of which is partial, in general, and dictates the volumetric content of the pore. Capillary effects when the interface fills the pore body are generally neglected. After complete occupancy of the pore body, the meniscus can invade a neighbouring pore throat if the corresponding capillary barrier is exceeded. Although pore network simulation has often been used in immiscible displacements (Lenormand *et al.*, 1988; Rege and Fogler, 1988; Blunt and King, 1991; Knight *et al.*, 1990), the simulation of bubble growth processes has only been recently attempted (Li and Yortsos, 1991). Consistent with these key rules, a pore network simulator was

developed by Li and Yortsos (1991), where both the flow field and the concentration field were computed following the above formulation. The particular details can be found in Li and Yortsos (1991). Here, we shall make use of the simulator to understand patterns and rates of growth.

### 3. GROWTH OF A SINGLE CLUSTER

The first problem to be considered is growth of a single cluster in a porous medium. The corresponding problem of growth in the bulk has been analyzed in great detail by many authors, following the seminal work of Scriven's (1959), where similarity solutions were developed for the problem corresponding to case (i). The bubble radius  $R$  was shown to follow the similarity scaling  $R \propto \sqrt{t}$ , the prefactor being proportional to  $\sqrt{Ja}$  at low  $Ja$ . Many other effects, including inertia, non-equilibrium thermodynamics etc., were also analyzed (Szekely and Martins, 1971; Szekely and Fang, 1973) and reviewed by Plesset and Prosperetti (1977).

In past works, bubble growth in porous media was also modeled using bulk models. For example, some authors (Moulu and Longeron, 1989; Kashchiev and Firoozabadi, 1993a, b) postulated that for case (i), single bubble growth in a porous medium also obeys the bulk growth similarity scaling. In addition, the further conjecture is often made that for case (iii), this similarity solution remains valid, leading to the new time scaling  $R \propto t\sqrt{a}$ , as the Jakob number is now time-dependent. In view of the previous discussion, such analyses should be viewed as overly simplified, since they ignore many aspects fundamental to porous media, such as non-compact patterns, which cannot be simply corrected by a shape factor, as typically done in effective media. Compact growth patterns are possible in *effective* porous media, such as Hele-Shaw cells, however, the growth and stability of which was analyzed recently (Li and Yortsos, 1994). In such structureless systems, the  $\sqrt{t}$  similarity scaling is obeyed, provided that capillarity is sufficiently strong to preserve radial symmetry.

To characterize single bubble growth in a porous medium requires that the two aspects of cluster *pattern* and its *rate of growth* be determined. We expect a *percolation* pattern for sufficiently small cluster sizes and a departure towards a *viscous fingering* pattern at larger sizes. Rates of growth depend on mass transfer, although the scaling exponents also depend on the particular pattern, thus on the competition between capillary and viscous forces as well. The boundaries that delineate these regimes were recently determined by Satik *et al.* (1995) but only for case (i) of a fixed supersaturation. As the growth of a single bubble under various conditions is necessary to understand the more complex multiple cluster problem, we proceed with a discussion of the problem and generalize the results of Satik *et al.* (1995) in the appropriate cases.

### 3.1. Single cluster growth pattern

Consider the growth of a single cluster in the three cases described above. The cluster follows a percolation pattern, if perimeter pore throats are invaded "one-at-a-time", such that the largest available bond is always invaded first. These rules are the same with *invasion percolation* in drainage, except that here, invasion occurs from an internal, rather than an external, source, and the possibility exists for many such internal sources (because of multiple nucleation sites). In this sense, the process is reminiscent of secondary imbibition at very low capillary numbers (Lenormand, 1990) or of vapor desorption in porous media (Yortsos and Parlur, 1989). Provided that the ratio in density between liquid and gas is sufficiently high, as is the case in typical applications, trapping of liquid occurs and should be included in the process.

The following conditions must apply for the existence of a percolation pattern: (1) Immediately preceding and during a pressurization step, all interfaces must be locked. This step concludes by the invasion of the largest among all available perimeter throats, when the filling step commences. (2) During a filling step, only one pore is filled and the simultaneous penetration of another throat is not possible. For instance, it is not possible that while the meniscus is in motion in some location,  $m$ , penetration occurs at another location,  $j$  [Fig. 1(b)].

The first condition is always satisfied, since during pressurization, the liquid pressure outside the cluster and the gas pressure inside the cluster are both spatially uniform (no flow). The second condition, however, relies on the magnitude of the viscous pressure drop. During the filling of a partly occupied pore  $m$ , the capillary pressure in the pore is small (taken equal to zero), thus  $P_g \approx P_{l,m}$ . For the simultaneous penetration of a perimeter bond at another location  $j$  requires  $P_g - P_{l,j} \geq 2\gamma/r_{ij}$  [Fig. 1(b)], namely that a sufficiently large viscous pressure drop must exist between pores  $m$  and  $j$ ,  $P_{l,m} - P_{l,j} \geq 2\gamma/r_{ij}$ . Conversely, if a percolation pattern is to be followed, the reverse inequality must be valid for any two such pores. This will be the case for sufficiently small cluster sizes. Sufficiently large pressure drops across the cluster, likely to increase with cluster size and with the capillary number, violate this constraint and lead to a different regime. Thus, although the pressure drop in the liquid does not affect significantly the interface concentration [see eq. (22)], it can be sufficiently large for viscous effects to be comparable to capillary forces and must be calculated. Inclusion of the flow field substantially increases the complexity of the numerical simulation.

When the pattern is of the percolation type, growth occurs by penetration of the largest size perimeter throat. Before this event, all interfaces are locked in place and a (relatively short) pressurization period elapses, during which, for cases (i) and (iii), mass transfer leads to the build-up of the gas pressure according to eq. (25). It must be pointed out that this

scenario is not true for case (ii), however, where the bubble grows at a constant rate and penetration of the largest perimeter throat is reached by a fast (instantaneous) decrease of the liquid pressure to the appropriate threshold, instead of the slow increase associated with the pressurization step. In all cases, upon the subsequent invasion of the largest perimeter throat, capillary pressure requirements relax and filling of the partly invaded pore continues following eq. (26), where volume expansion must also be considered.

The other distinct pattern corresponds to rates of growth and cluster sizes sufficiently large, such that viscous forces dominate. In this regime, capillarity is negligible and adjacent pores are invaded at the relative rates determined from the flow-field determined condition (A1). Here, the problem reduces to the standard displacement of a liquid by a gas. The corresponding pattern is of the viscous fingering-type and should share many of the diffusion-limited aggregation (DLA) properties typically assigned to such patterns [see also Li and Yortsos (1994) for a detailed discussion of this instability]. While the effect of mass transfer in either percolation or viscous fingering regimes is mainly on the rate of growth, mass transfer may also affect the pattern characteristics during the transition between these regimes.

The transition from a percolation to a viscous fingering pattern begins when more than one perimeter pore is invaded or become partly occupied. Numerical simulations and a scaling study were conducted to demarcate this percolation boundary. Because of excessive computational requirements, all simulations were conducted in relatively small (or  $50 \times 50$ ) networks. Typical simulation patterns are shown in Fig. 3. The pattern is strictly percolation [Fig. 3(a)] if the cluster radius of gyration  $R$  is smaller than a critical size  $R^p$ . Otherwise, more than one pore can be invaded at the same time and a purely percolation pattern ceases to exist. For sufficiently large sizes ( $R > R^p$ ), the patterns tend to the characteristic viscous fingering pattern [Fig. 3(b)]. Both  $R^p$  and  $R^p$  were found to decrease with an increase in the capillary number, namely with an increase in  $D$ ,  $\mu$  and  $Ja$  in case (i),  $\mu$  and  $Q$  in case (ii),  $D$ ,  $\mu$ ,  $a$  and  $t$  in case (iii), and with a decrease in  $\gamma$  and  $k$  in case (i),  $\gamma$  in case (ii), and  $\gamma$  and  $P_0$  in case (iii), respectively [where in the above we took  $l^* \sim r^*$ , and  $k \sim (r^*)^2$ ]. For fixed values of  $S$ , the two boundaries,  $R^p$  and  $R^p$ , are a single function of  $Ca$  (Fig. 4). However, an increase in  $S$  for the same  $Ca$  leads to lower critical values, due to increased effects of convection. We should note that the boundaries in Fig. 4 correspond to rather high capillary numbers, because of the small cluster sizes involved due to the small computational domains. For larger cluster sizes, the transition between regimes occurs at lower (and more realistic) capillary numbers. Such an extrapolation of the limiting curve can be provided by a scaling analysis (Satik *et al.*, 1995).

The existence of critical cluster sizes can be anticipated from the previous work on the capillary and

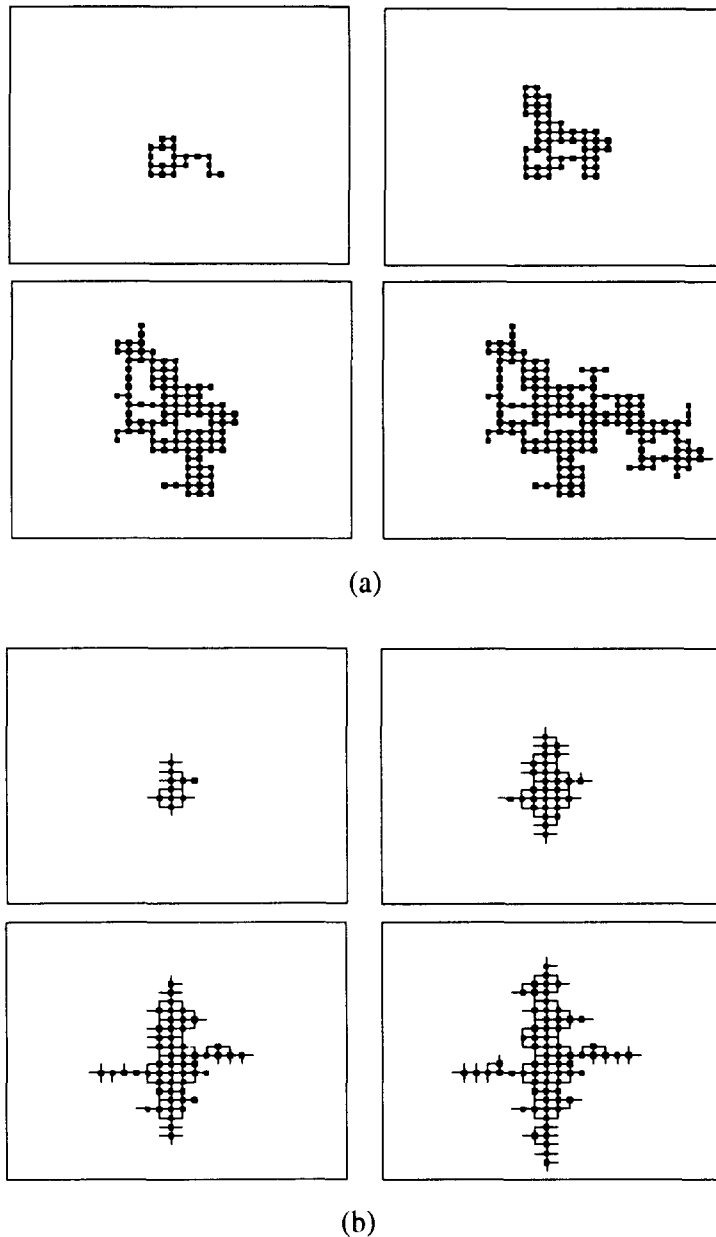


Fig. 3. Snapshots of simulated single cluster growth under conditions of (a) capillary control and (b) viscous control.

viscous fingering regimes by Lenormand (1989), except that here mass transfer must be additionally considered. In a companion paper, we have proposed such a scaling theory (Satik *et al.*, 1995) for case (i) to interpret the numerical findings of Fig. 4. It was shown that for case (i) and under the assumption that the concentration field is quasi-static,  $S \ll 1$ , the percolation boundary in a 3-D system scales as

$$\left(\frac{R^p}{r^*}\right)^{1/\nu+1} \frac{\alpha Ca}{\sigma} \sim \text{const} \quad (27)$$

where  $\sigma$  is the standard deviation of the pore size distribution and  $\nu$  is the exponent of the correlation

length in percolation [ $\nu = 0.88$  in 3-D, Stauffer (1985)]. A different result involving logarithmic corrections was found for 2-D growth

$$\left(\frac{R^p}{r^*}\right)^{1/\nu} \left(\frac{\ln \frac{R^p}{r^*}}{\ln \frac{R_e}{R^p}}\right) \frac{\alpha Ca}{\sigma} \sim \text{const} \quad (28)$$

where  $R_e$  denotes the outer boundary of the medium, assumed radially symmetric. The same scalings are also expected for case (iii) except that it must be kept in mind that  $Ca$  is time-dependent. However, to determine the scaling of the percolation boundary with the

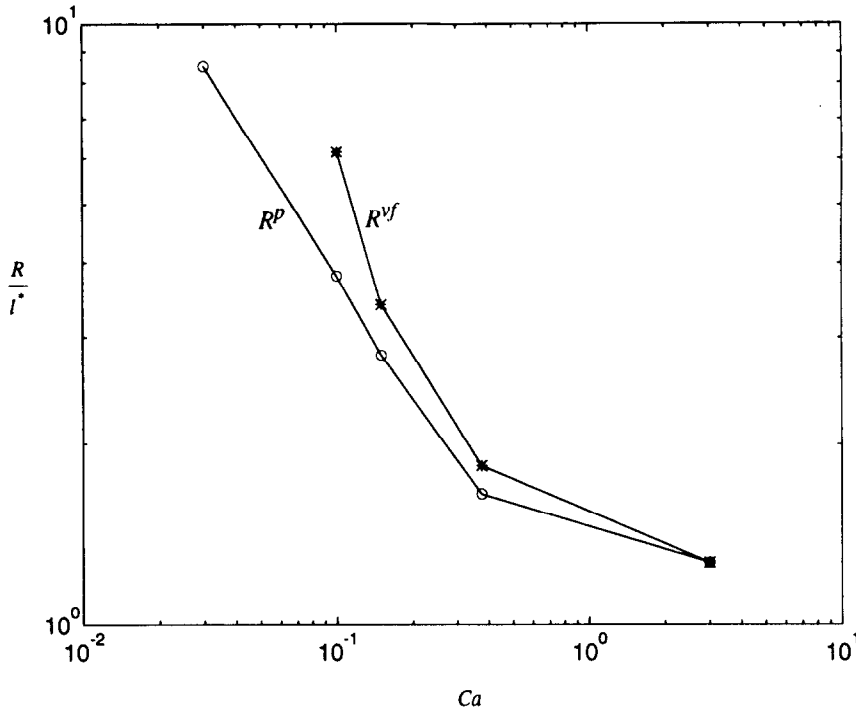


Fig. 4. Percolation and viscous fingering boundaries from simulations in a 50 × 50 square lattice.

pressure decline rate for case (iii) the rate of growth must also be determined, as discussed below.

Analogous results were found for the boundary that demarcates the transition from a purely DLA pattern to a percolation regime. For example, the corresponding equation in 3-D geometries reads (Satik *et al.*, 1995)

$$\left(\frac{R^{vf}}{r^*}\right)\left(\frac{\alpha Ca}{\sigma}\right) \sim \text{const} \quad (29)$$

with logarithmic corrections necessary for 2-D geometries. These theoretical results were found in qualitative only agreement with the simulations of Fig. 4 due to the strong finite size effects. Computational limitations do affect the accuracy of these non-local problems, where concentration and pressure fields must be calculated (Li and Yortsos, 1991).

Somewhat different scalings are obtained for case (ii). Here, mass transfer is not relevant in setting the viscous forces, and the percolation boundary is

$$\left(\frac{R^p}{r^*}\right)^{1/\nu} \frac{Ca'}{\sigma} \sim \text{const} \quad (30)$$

where the modified capillary number,  $Ca' = Q\mu/\gamma r^*$ , was introduced, and similarly for the viscous boundary.

It must be remarked that in the transition towards a purely viscous fingering regime, the viscous forces across the cluster may be sufficiently strong to cause the mobilization of the entire cluster. For example, cluster mobilization is possible for sufficiently large cluster sizes in the presence of gravity (Dumoré, 1970).

Because mobilization is the result of viscous forces across the cluster exceeding the capillary forces, this boundary is expected to be parallel to the percolation boundary. Cluster mobilization could have important ramifications on the definition of the critical gas saturation.

### 3.2. Rates of growth

The second important aspect in the characterization of bubble growth is rates of growth. As pointed out previously, compact bubble growth obeys the similarity scaling  $R \propto \sqrt{t}$  under the following conditions: 3-D growth in the bulk or in an effective porous medium for case (i), or 2-D growth in an effective porous medium (Hele-Shaw cell) for case (ii). In the 3-D case, this is the result of the scalings  $V \sim R^3$  and  $dn_k/dt \sim R$ , from which the  $\sqrt{t}$  scaling follows.

Consider now the rate of growth in a 3-D porous medium. Because of the fractal patterns involved, the scaling of volume to the radius of gyration obeys a different expression

$$\frac{V}{(r^*)^3} \sim (R/r^*)^{D_f} \quad (31)$$

where  $D_f$  is the fractal dimension of the gas cluster (equal to 2.5 for both a 3-D percolation cluster and a 3-D DLA cluster). Expression (31) is valid provided that the cluster size is sufficiently large for the power law to apply (otherwise finite-size effects must also be included). To calculate the rate of growth requires an expression for the mass transfer. As before, we consider the case of quasi-static diffusion. For cases (i)

and (iii), solving eq. (21) at  $S \ll 1$  and substituting the results in eqs.(26) and (31), yields the following expression:

$$\left(\frac{R}{r^*}\right)^{D_f-1} = \frac{4\pi\alpha(D_f-1)}{D_f} \tau \quad (32)$$

where we take without loss  $l^* = r^*$ . In terms of time  $t$ , the cluster grows according to the scaling

$$R \sim (Jat)^{1/(D_f-1)} \quad (33)$$

for case (i), and

$$R \sim \left(\frac{at^2}{P_0}\right)^{1/(D_f-1)} \quad (34)$$

for case (iii), respectively. Evidently, as a result of its ramified structure, the cluster grows faster ( $R \sim t^{2/3}$  or  $t^{4/3}$ ) than in its effective medium analogue (which is  $R \sim t^{1/2}$  or  $t$ ), in the two cases, respectively. The corresponding expressions for the rate of growth in a 2-D medium must include logarithmic corrections (Satik *et al.*, 1995)

$$\left(\frac{R}{r^*}\right)^{D_f} \left(1 + D_f \ln \frac{R_e}{R}\right) = 2\pi\alpha D_f \tau \quad (35)$$

where we again assumed  $l^* = r^*$ , and where  $D_f = 1.89$  for 2-D percolation and  $D_f = 1.70$  for 2-D viscous fingering. Analogous expressions that also include effects of convection (larger  $S$ ) have not been derived and they are currently under study. Again, case (ii), where a constant growth rate is imposed, has a differ-

ent scaling

$$R \sim (Qt)^{1/D_f} \quad (36)$$

for any dimension and  $Q$ . These are all different from the  $\sqrt{t}$  scaling corresponding to an effective medium.

Having the information on the rate of growth, the scaling of the critical size of the percolation boundary  $R^p$  in terms of the pressure decline rate  $a$  for case (iii) can be obtained. By eliminating time between the expression for the supersaturation and the rate of growth, one can readily show the result

$$\left(\frac{R^p}{r^*}\right) \sim \left(\frac{ar^{*2}}{DP_0}\right)^{-v/[v(1+D_f)+2]} \quad (37)$$

which suggests a straight line with slope  $-v/[v(1+D_f)+2]$  in the appropriate log-log plot. This is consistent with the numerical trends obtained with the pore network simulator as shown in Fig. 5.

We conclude that during single bubble growth in a porous medium the following regimes develop in succession: a short duration early-time regime, where finite size effects dominate (e.g.  $R/r^* \equiv R_D < 10$ ), the growth is still compact and the effective medium scaling  $R_D \sim t^{1/2}$  applies; a percolation regime ( $10 < R_D \leq R_D^p$ ), where the gas bubble is a percolation cluster and the scaling follows from the above using the fractal dimension of the percolating cluster; a transition towards a viscous fingering regime ( $R_D^p < R_D < R_D^{vf}$ ); and a viscous fingering regime ( $R_D^{vf} < R_D$ ), where the scaling changes according to

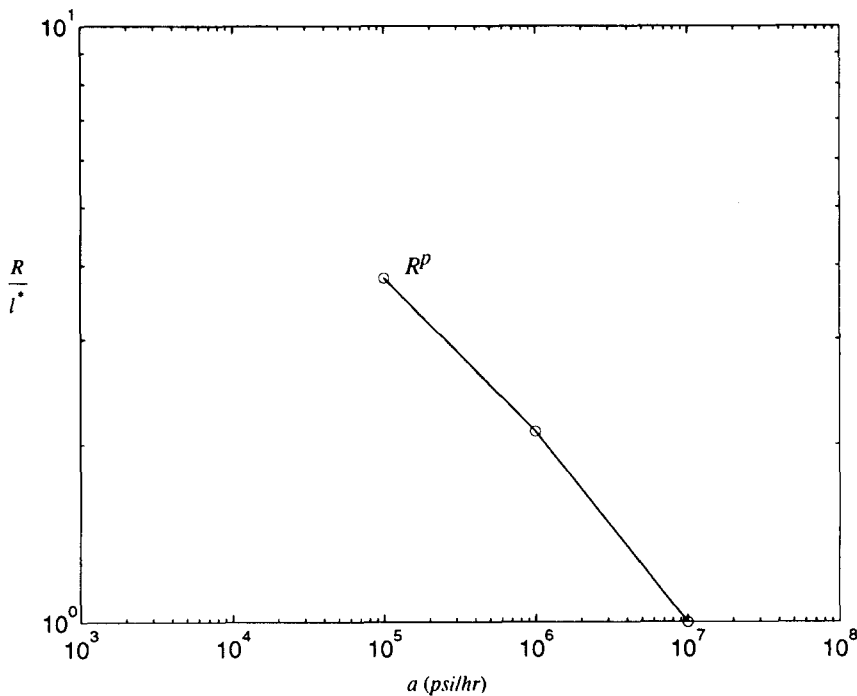


Fig. 5. Effect of pressure decline rate on the percolation boundary from simulations in a  $30 \times 30$  square lattice.

the viscous fingering fractal dimension. The percolation and viscous fingering limiting sizes,  $R_D^p$  and  $R_D^{ef}$ , respectively, depend on  $Ca$  and  $S$ .

All the above predictions are valid under the assumption that mass transfer occurs by quasi-static diffusion. For compact patterns (bulk growth) under the conditions of case (i), the appropriate condition is readily shown to be  $Ja \ll 1$ , uniformly in time. However, this is not necessarily true for the case of fractal patterns either for case (ii) or (iii), where the supersaturation is time-dependent. The validity of the condition in these cases is examined in Appendix B, where it is shown that the bulk condition can still be used to denote mass transfer dominated by quasi-static diffusion when the above percolation and viscous fingering boundaries are reached. When the quasi-static approximation fails, a different scaling would result. At present such a scaling theory is not available.

#### 4. GROWTH OF MULTIPLE CLUSTERS

As pointed out previously, at typical conditions, growth of the gas phase occurs from multiple sites, each of which is generally activated at each own supersaturation [dictated by capillary and geometrical characteristics of the type shown in inequality (1)]. Given a distribution of sites, several important issues arise, for example the competition between growing clusters, the ensuing patterns and rates of growth, the prediction of site activation in terms of the parameters of the system and, ultimately, the determination of the critical gas saturation.

Before we proceed with the analysis of multiple cluster growth, we must note that the competition between growing clusters in a porous medium is different than in the bulk, where, under quasi-static conditions, it is often described by *Ostwald ripening*. The latter is based on the solubility dependence on curvature and predicts the growth of larger bubbles at the expense of smaller ones. Because it relies on the direct proportionality between bubble size and radius of curvature, which is indeed obeyed in the bulk, however, *Ostwald ripening* is of less relevance to porous media, where cluster size and capillarity are weakly, if at all, coupled. In porous media, the competition between growing clusters is controlled by the pore structure and by mass transfer, thus the solubility dependence on radius is less important.

To characterize the multiple cluster problem, a measure of the cluster volumetric density must be introduced. We shall define the *nucleation fraction*,  $f_q(t)$ , which is the number fraction of sites which have been activated at time  $t$  and around each of which a cluster has grown. Assuming that the site activation can be modeled as in expression (1), we can assign a distribution  $F(W)$ , much like a pore size distribution  $\alpha(r)$ , to all the pores of the porous medium (Fig. 6) (where only the largest among possibly many such cavities will be considered in a given pore). This distribution  $F$  is expected to have a mean much smaller than the average pore size, so that the majority of the pores do not become activated. The cavity size distribution is useful in estimating the nucleation fraction,

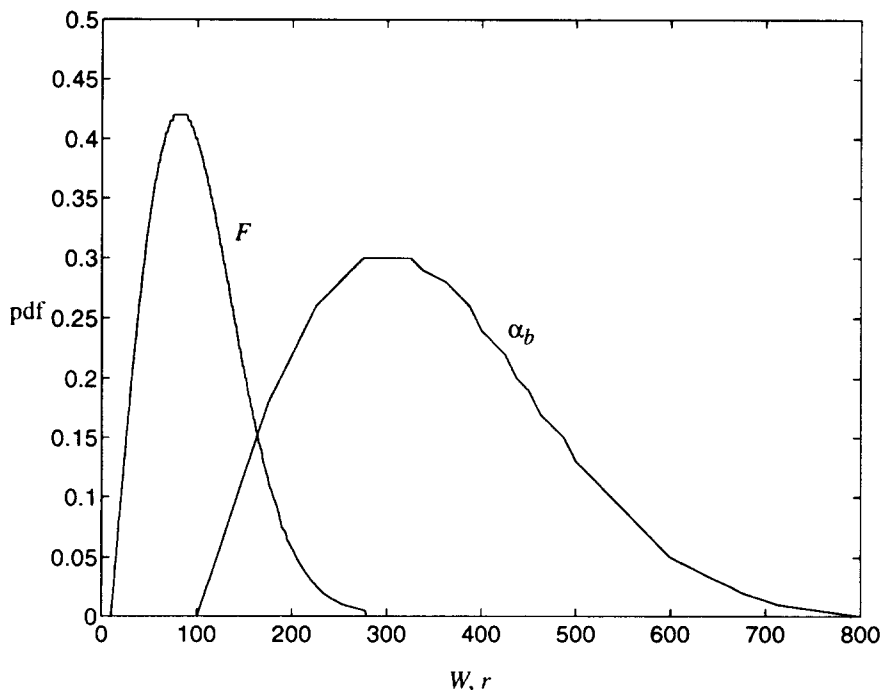


Fig. 6. Schematic of probability distribution functions (pdf) for nucleation cavity  $F(W)$  and pore throat size  $\alpha_b(r)$ .

particularly for the case of slow growth, where concentration gradients are small. Then,  $f_q(t)$  can be calculated as a function of the prevailing supersaturation  $\Delta P(t)$ , from the following simple expression:

$$f_q = \int_{2\gamma/\Delta P(t)}^{\infty} F(W) dW. \quad (38)$$

To actually compute  $f_q(t)$  in the general case, however, requires the solution of the entire problem and a knowledge of the site distribution. In the absence of any information, the location of nucleation sites and their activation thresholds must be considered as random variables.

The existence of multiple nucleation sites introduces a new characteristic length in the system, which for a 3-D geometry is

$$l_q \sim \frac{r^*}{(\phi f_q)^{1/3}}. \quad (39)$$

This length sets the minimum spacing between centres of growing clusters at any given time and denotes the appropriate diffusion scale for the system (thus, in the multiple cluster problem one can take  $l^* \sim l_q$ ). In describing multiple cluster growth, we shall examine cluster growth patterns and rates of growth.

#### 4.1. Growth patterns

Assume that at any given time there exist multiple nucleation centers, with cluster sizes sufficiently small for each cluster to grow following a *percolation* pattern. The percolation boundary previously developed for a single cluster should be applicable here as well: the existence of multiple clusters slows down mass transfer due to screening effects, while at the same time the mass that reaches each cluster is less than in the single cluster problem, since more pores are competing for the same amount of solute. As a result, viscous pressure drops are also smaller. Thus, for each cluster to remain in the percolation pattern regime, namely for it to grow by invasion of the largest throat in its perimeter, the condition  $l_q < R^p$ , where  $R^p$  is evaluated from the single cluster expression, should be sufficient on the average. Because of expression (39), this condition can be translated into one on the nucleation fraction

$$f_q \geq \frac{8}{\phi [R_b^p(Ca, S)]^3} \quad (40)$$

where the normalized critical size  $R_b^p(Ca, S)$  is a function of  $Ca$  and  $S$ , as described in Section 3. For typical values of  $Ca$ ,  $S$  and  $f_q$ , this condition should be well obeyed. Thus, in the remainder of the paper, we shall proceed with the assumption that all clusters individually grow by following percolation rules *locally* and neglect any viscous effects on the pattern.

It follows that given the various clusters (or their mother activation site) and the porous medium geometry, the *sequence*, but not the *rate*, of pore throat invasion of each cluster is fixed. In view of the previous theory, a cluster would either be in a pressur-

ization stage, during which all menisci are locked and the gas pressure is in the process of increasing for the penetration of a subsequent throat, or in a filling stage, during which a meniscus advances in the newly occupied pore. Although the percolation rules are followed *locally* for each cluster, however, they are not necessarily followed *globally*. In fact, three different patterns can be identified as described below.

(1) *Global percolation*: At any given time, we may arrange the throats in the perimeter of *all* clusters in a sequence of decreasing sizes, e.g.  $T_1, T_2, T_3, \dots, T_n$ . We shall call the pattern a *global percolation* pattern if  $T_1$  is always the next throat to be penetrated, regardless of the size or the location of the particular cluster of which this throat becomes part. It will be shown below that this is possible at low pressure decline rates.

For a global percolation pattern to be possible, either all clusters must be in a pressurization stage or only one cluster must be in a filling stage. This condition can be fulfilled only if the mass transfer rates to the non-growing clusters become negligibly small sometime during the filling stage, so that their pressure stabilizes. For this to be true, in turn, requires that the corresponding interface concentrations rapidly become equal to the far-field concentration,  $C_\infty$ . Consider, for example, two clusters, one filling ( $f$ ) and one pressurizing ( $p$ ) and denote by  $C_f$  and  $C_p$  their respective interface concentrations. Assuming negligible viscous pressure drop, we can readily show that the following holds:

$$C_p \leq C_f + \frac{2\gamma}{Kr_p} \quad (41)$$

where  $r_p$  is the size of the largest perimeter pore throat of the pressurizing cluster. For the clusters to remain in their respective stage until the completion of the filling of cluster  $f$ , and in view of the fast mass transfer during the pressurization step alluded to in expression (A3), requires  $C_p \approx C_\infty$ . Because we also have  $C_f = P_\infty/K$ , inequality (41) implies  $KC_\infty - P_\infty \leq 2\gamma/r_p$ . In other words, for a global percolation pattern to be possible, the supersaturation in the system,  $KC_\infty - P_\infty$ , must be sufficiently weak compared to the capillary pressure level. A necessary condition for this is supersaturation *depletion*, namely  $C_\infty$  must decrease with time sufficiently fast. For case (iii) this is likely to be true at sufficiently low decline rates. Depletion of supersaturation occurs because of the finite size of a system involving multiple growing clusters.

Based on these ideas, the following condition for a global percolation pattern can be derived as shown in Appendix C:

$$a \ll \frac{D\gamma}{(r^*)^3} (\phi f_q)^{1-1/D_f} \alpha^{1/D_f}. \quad (42)$$

This condition sets an estimate for global percolation conditions to apply. Expression (42) is an improved version of a previous heuristic result derived by Yor-

tsos and Parlár (1989) and sets an estimate on the upper limit of  $a$ . Because  $r^*$  is proportional to  $\sqrt{k}$ , the condition is likely to be applicable to lower permeability media. It is also favored at conditions of high capillarity and a relatively high nuclear fraction.

The existence of a global percolation regime is very useful, for the order of site occupation is predetermined, given the nucleation characteristics of the porous medium. The full problem can be solved, including the sequence of pore occupancy, the sequence of site activation (assuming their characteristics are precisely known) and the nucleation fraction evolution, the evolution of gas saturation as a function of pressure and time, and the magnitude of the critical gas saturation, as discussed later in this paper.

When global percolation is not followed, any two clusters may be at different stages. For example, while cluster  $i$  is at a pressurization step, cluster  $j$  may be at a filling step and *vice versa*. Thus, the exclusivity condition of "one-pore-at-a-time" will not hold, except at conditions of global percolation. Now, growth occurs simultaneously in the various clusters, which compete for the available solute. For example, in the case where two clusters are simultaneously in a pressurization stage, the cluster that grows next may not be the one with the largest perimeter throat but the one where mass transfer is highest. The exception is case (ii) involving growth at a constant rate, where if all clusters are temporarily frozen, subsequent penetration takes place by a reduction of the liquid pressure to the level necessary for the throat with the least overall capillary pressure threshold to be invaded. In general, however, the simultaneous lock of all clusters is rather unlikely in view of expression (A3): As long as the ratio  $P_c/P_l$  and the cluster sizes remain small enough,  $\Delta t_p$  cannot exceed  $\Delta t_f$  by an order of magnitude, as would be required for the rapid filling of all clusters. Thus, the order by which pore throats in different clusters are invaded is not solely dictated by capillarity alone but is also affected by the rates of mass transfer. Contrary to the single cluster problem, mass transfer affects the growth patterns in the multiple cluster problem. Two such patterns are discussed below.

(2) *Percolation-DLA*: Assume that all nucleation sites have been activated at the onset of the process (instantaneously) and no further nucleation is possible. For example, this is possible under the conditions of case (i) of fixed supersaturation, or in the early stages of case (iii) at relatively high decline rates, where the supersaturation has not been depleted. Given the location of the nucleation sites, mass transfer rates can be computed for each cluster, the subsequent growth of which is obtained from eq. (25) with the penetration sequence in each cluster satisfying percolation rules. Furthermore, under the assumption that the mass transfer is quasi-static, the concentration field is reduced to the solution of the Laplace equation

$$\nabla^2 C_D = 0 \quad (43)$$

subject to the boundary conditions

$$C_{D,\infty} = 1 \quad \text{in the far-field} \quad (44)$$

$$C_D = 0 \quad \text{at the cluster interfaces} \quad (45)$$

the latter arising from eq. (22) in the limit of small  $\Pi_1$ . We shall denote this as a *percolation-DLA* pattern. Indeed, this problem involves an interesting combination of *DLA* rules for computing the mass transfer and of *percolation* rules for advancing each cluster. This pattern can be equivalently computed without the need of a detailed simulator, by using the following simple algorithm: From random sites at the boundary of the computational grid, a number  $M$  of random walkers are launched, which terminate their walk when any cluster is encountered. Each cluster grows by occupying the largest size perimeter throat available to it per local percolation rules. However, the rate of growth of a cluster  $k$  is taken to be in proportion to the flow  $M_k$  of walkers it receives in this internal

$$\frac{dV_{Dk}}{dt_D} \sim \frac{M_k}{M}. \quad (46)$$

It should be pointed out that contrary to the classical *DLA* cluster, each individual cluster here is of the percolation type. However, the overall pattern is not the global percolation discussed previously, but a different pattern determined from the solution of the mass transfer (*DLA*) problem. Furthermore, although clusters near the boundary are likely to receive a larger mass flux and to grow accordingly faster, the random location of the pore to be invaded next, as a result of local percolation, weakens substantially the usual screening and shielding effects associated with *DLA* processes. This enables clusters away from the system boundary to grow, despite their disadvantageous position. A comparison of the statistical algorithm with the numerical solution of the full problem shows an excellent agreement. Patterns typical of this regime are shown in Fig. 7, where  $M = 2000$  and the computational size is  $30 \times 30$ . Figure 7(a) shows the numerical simulation results with the fixed concentration,  $C_{D,\infty} = 1$ , prescribed at the boundaries, while Fig. 7(b) shows the results simulated with the *DLA* algorithm. The two methods give very similar results. Because the statistical analogue works well only for the boundary condition  $C_{D,\infty} = 1$ , however, this model should be a good approximation only for processes at a constant supersaturation. When used for case (iii), the model is successful at the early stages, but it becomes progressively worse when substantial supersaturation depletion commences.

(3) *Percolation-modified DLA*: The most general pattern at conditions of capillary control involves the constant pressure decline relate case (iii), but at rates higher than expression (42), such that although the supersaturation is being depleted, it remains higher than the capillary pressure level. The prototypical problem here involves growth of multiple clusters in a finite system (e.g. a square network in 2-D), at one

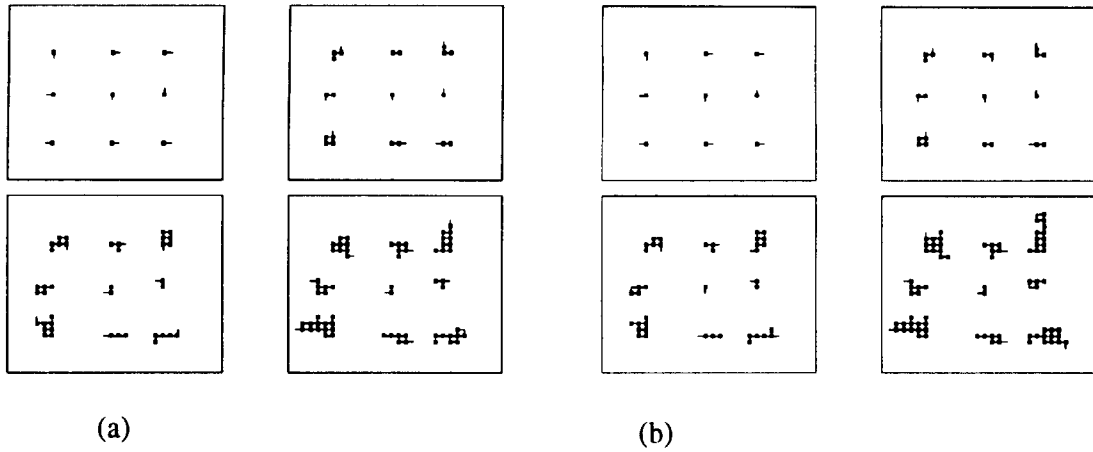


Fig. 7. Comparison of patterns for case 1 (percolation-DLA): (a) numerical simulation; (b) percolation-DLA algorithm.

side of which the pressure declines at the prescribed rate, the other sides being no-flow boundaries. Even though we may still take weak supersaturation,  $S \ll 1$ , the problem cannot be solved by considering the quasi-static limit  $\nabla^2 C_D = 0$ , which, for a finite system, has the trivial solution  $C_D = 0$  (assuming  $\Pi_1 \ll 1$ ). Instead, it requires the full consideration of the transient and convective terms in eq. (21), which, because of their dependence on the flow field, make it equivalent to solving the full problem. Nonetheless, a simplified model that describes cluster competition can be developed by neglecting convection, but by retaining the transient terms. With this assumption, which retains the supersaturation depletion, eq. (21) yields

$$\frac{\partial}{\partial \tau} [(C_D - 1)S] = \nabla^2 C_D \quad (47)$$

$$C_D = 0 \quad \text{at cluster boundaries} \quad (48)$$

$$\frac{\partial C_D}{\partial n} = 0 \quad \text{at system boundaries.} \quad (49)$$

For case (iii), the system admits the *separable* form solution

$$C_D = 1 + \frac{(aI_q^2/DP_0)G(\mathbf{x}) - S}{S} \quad (50)$$

where  $G(\mathbf{x})$  is only spatially and configuration-dependent and is given from the solution of the following problem:

$$\nabla^2 G = -1 \quad (51)$$

$$G = 0 \quad \text{at cluster boundaries} \quad (52)$$

$$\frac{\partial G}{\partial n} = 0 \quad \text{at system boundaries.} \quad (53)$$

Equation (51) represents a steady-state reaction-diffusion problem with a constant source term equal to 1, with perfect sinks at the cluster boundaries and with

no-flux condition at the system boundaries. We shall call the resulting pattern, the *percolation-modified DLA* pattern. As before, a statistical analogue for this problem is also possible and involves a random walk. Here, however, the walkers originate at *random* points in the liquid, contrasted to the previous pattern where they are launched from the boundary. As in the previous model, the growth of the clusters is taken in proportion to the flow of walkers they receive. Also as in the previous problem, however, the exact mapping to actual time and pressure is not possible with such an approach.

Growth patterns obtained by the numerical solution of the full problem, including convection, for a constant pressure decline rate and an initially fixed nucleation fraction are shown in Fig. 8(a). Compared with the pattern obtained from the simulation of the full problem, the modified DLA results [Fig. 8(b)] are similar at early times (or at low nucleation fractions), but they deviate somewhat from the numerical simulation when the cluster density increases. If progressive nucleation is included, additional sites will be activated, the growth of which changes somewhat the dynamics of the process and the patterns obtained. This analysis is still in progress. Percolation-modified DLA patterns differ significantly, however, from percolation-DLA patterns (Fig. 7).

We conclude this section by commenting on the growth patterns of case (ii) of constant liquid withdrawal rate. As previously noted, the supersaturation is likely to be highest at the beginning of the process, during which time nucleation would be completed. Global percolation requires that viscous pressure drop is negligible compared to the capillary pressure and the growth rate is sufficiently large so as not to allow for significant mass transfer in the pressurizing cluster. The second condition can be determined following arguments similar to those for case (iii). During the time interval it takes for the growing cluster to

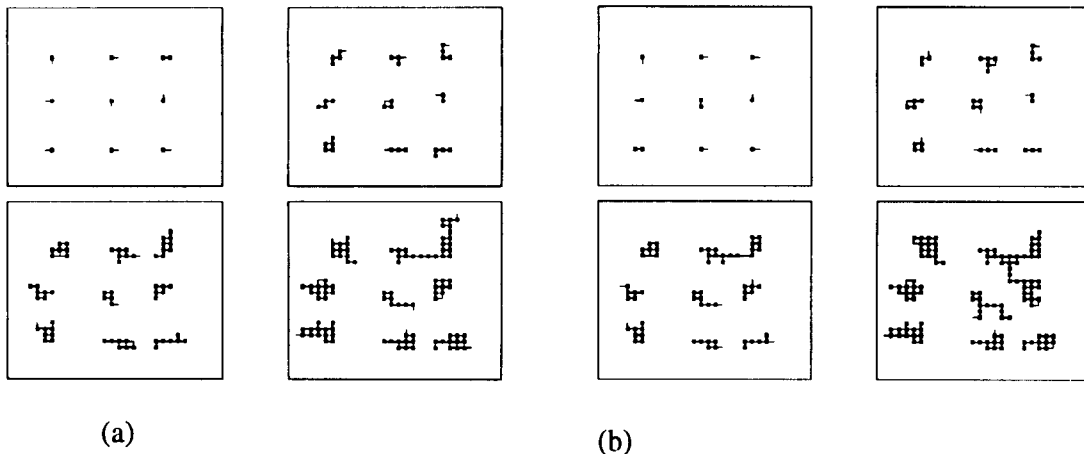


Fig. 8. Comparison of patterns for case 2 (percolation-modified DLA,  $a = 1$  psi/h): (a) numerical simulation; (b) percolation-modified DLA algorithm.

complete a filling step,  $\Delta t = V_s/Q$ , the pressure of the pressurizing cluster has increased by the increment

$$\Delta P \sim \left(\frac{V_s}{QV_k}\right)\left(\frac{\mathcal{R}T}{M_w}\right)4\pi R_k SD \quad (54)$$

where the quasi-static approximation was used for mass transfer. For a rough estimate we may further approximate  $R_k$  by the nucleation length  $l_q$  and make use of expression (B6) to yield the approximate condition

$$P_0 < \frac{2\gamma}{r}\left(\frac{l_q}{r}\right)^{D_f} \quad (55)$$

Clearly, this can only be satisfied at very small nucleation fractions and/or at high capillary pressures.

4.2. Rates of growth

The evolution of the gas saturation as a function of time is trivial for case (ii), but of considerable interest for the other two cases, in particular for case (iii). Here, because of the correspondence between pressure and time, gas saturation and pressure are also in one-to-one correspondence, with the pressure decline rate as a parameter. Simple results are possible for the case of low pressure decline rates, where global percolation applies. During this process, the sequence of pore occupancy is known *a priori*. The sequence of pore occupation dictates the gas saturation level, which is in turn related to the system pressure. Because of the assumed weak supersaturation levels, concentration gradients are small, and the integral balances for solute and total mass read

$$M_w dn + V_T d[C_\infty(1 - S_g)] + C_\infty dV_l = 0$$

$$- V_T dS_g + dV_l = 0. \quad (56)$$

After some manipulations, we obtain the following relation between pressure and gas saturation,  $S_g$ :

$$\frac{P_t}{P_0} = \left(1 - S_g + \frac{S_g}{\alpha}\right)^{1/(\alpha-1)} \quad (57)$$

based on which the time evolution of  $S_g$  is determined. It is evident that as the solubility constant  $K$  increases, the gas saturation decreases [Fig. 9(a)]. The rates of growth are directly obtained from eq. (57) by substituting for the pressure

$$S_g = \left(\frac{\alpha}{1 - \alpha}\right)\left[\left(1 - \frac{at}{P_0}\right)^{\alpha-1} - 1\right] \quad (58)$$

as shown schematically in Figs 9(a) and (b). As expected, the effect of the pressure decline rate is to lead to an increase in the gas saturation at a fixed time. However, in this regime,  $S_{gc}$  is only a function of the nucleation fraction, independent of  $a$ . This scaling applies at pressure decline rates sufficiently low for the pattern to be at conditions of global percolation. Because the latter requires a non-trivial nucleation fraction, eq. (58) is expected to be applicable only during the latter stages of the process, the earlier part being approximately described by the single cluster growth rate expression (34). For a given pressure decline rate, the transition from expressions (34) to (58) occurs earlier at higher nucleation fractions.

When the pattern is a combination of local percolation and mass transfer [type (2) or (3) discussed previously], an analytical scaling of the saturation with time cannot be obtained. Although the early time growth still obeys the scaling (34), the subsequent rates of growth cannot be simply obtained and the full numerical solution of the problem is necessary. We have examined the sensitivity of the rate of growth on the following parameters: (a) pressure decline rate at a fixed nucleation fraction, all sites activated at the onset of the process; (b) pressure decline rate at a fixed sequence of activation sites, each activated at a specified supersaturation; (c) nucleation fraction at a fixed pressure decline rate, with all sites activated at the onset of the process. Typical results are shown in Figs 10–12 for the conditions of gas growth from carbonated water saturated at 72 psia. Shown in Fig. 10(a) is the sensitivity of the  $S_g$  vs  $t$  curve for case (a)

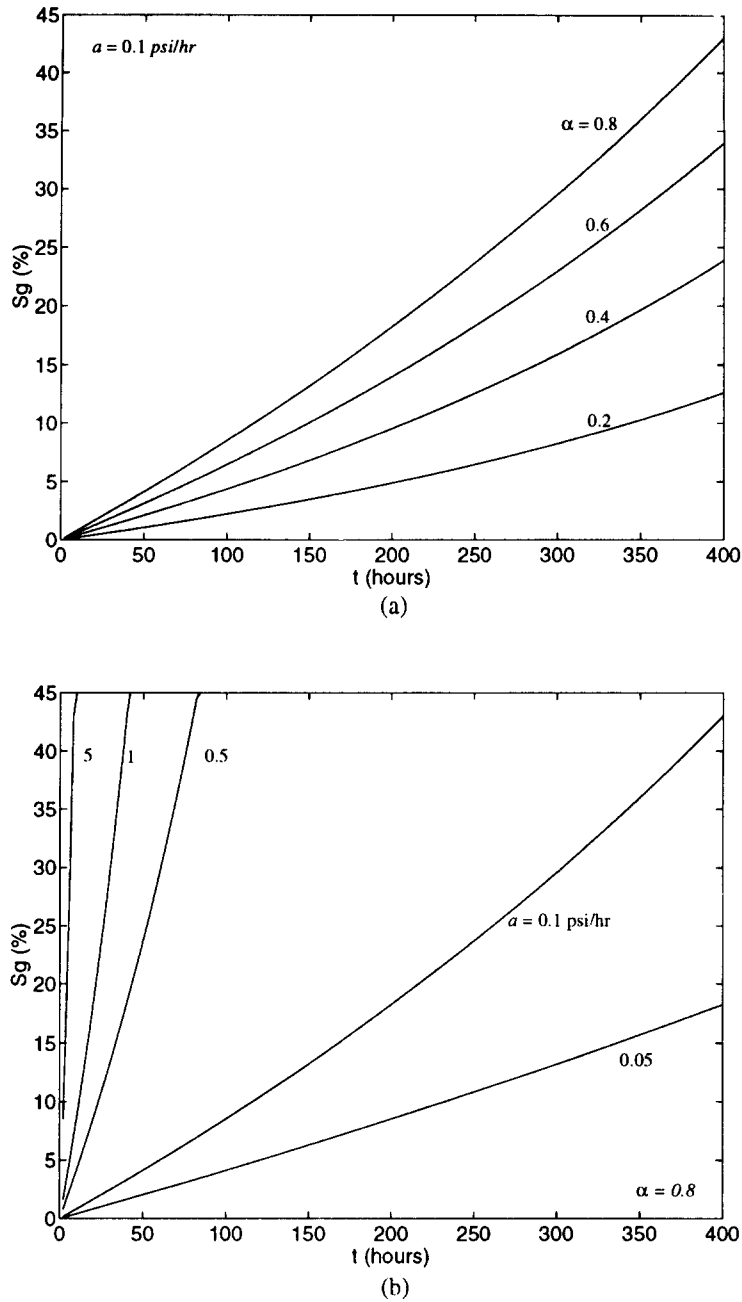


Fig. 9. Evolution of gas saturation vs time for global percolation: (a) effect of solubility parameter  $\alpha$ ; (b) effect of pressure decline rate  $a$ .

involving 16 nucleation sites. As the pressure decline rate increases, the gas saturation at a fixed time (or equivalently at a lower pressure) increases. This effect is also observed when the global percolation model is used [eq. (58)]. A different representation of this is shown in Fig. 10(b), where the variation of the pressure-saturation curve is plotted in terms of the pressure decline rate. The overall effect is the consistent lowering of the saturation corresponding to a given pressure as  $a$  increases. Because in this region the pressure-saturation curve is sensitive to  $a$ , the satura-

tion does not scale uniquely with the product  $at$ , as in the case of global percolation.

When the nucleation fraction is not fixed at the beginning of the process, but each site is activated at a prescribed supersaturation [case (b)], the effect of the pressure decline rate remains the same, higher values of  $a$  leading to higher saturations at a fixed time [Fig. 11(a)], and to lower saturation at a fixed pressure [Fig. 11(b)]. In this simulation, successive sites were activated at intervals of 1 psi, for a total of 40 activated sites. Finally, the effect of the nucleation

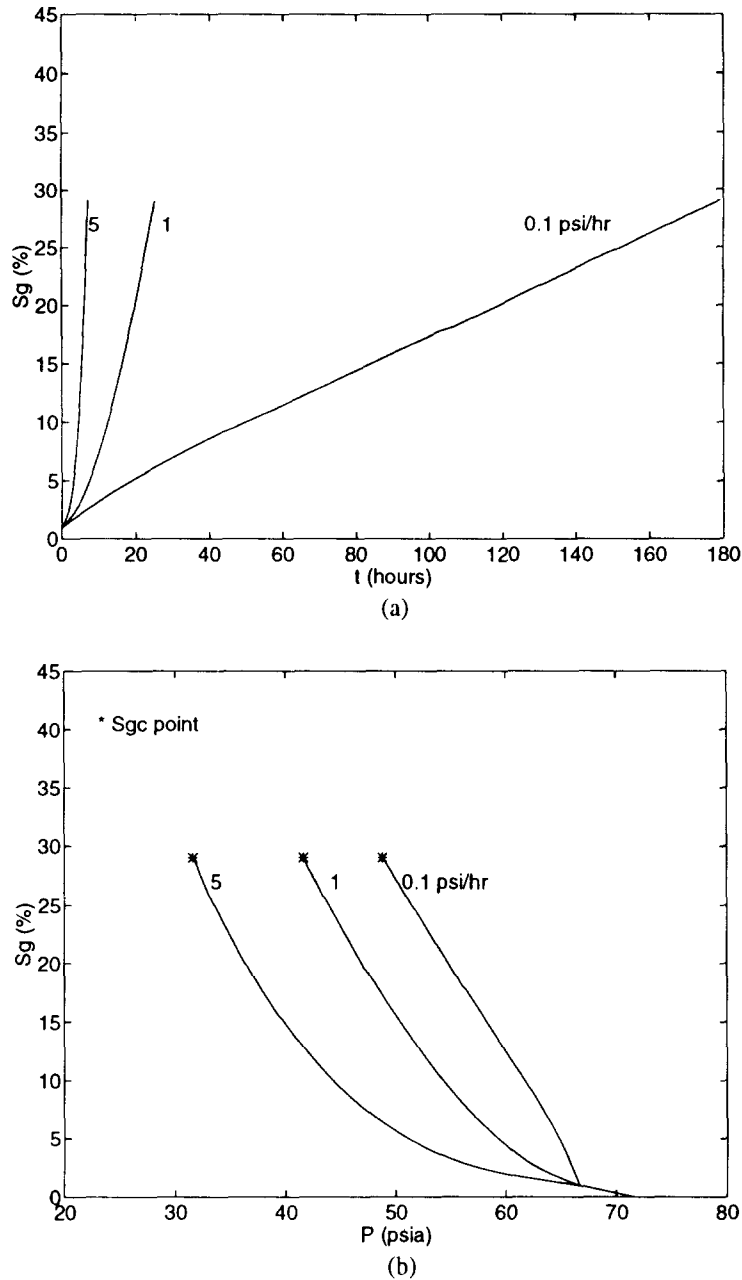


Fig. 10. Simulation of the evolution of gas saturation at a fixed nucleation fraction ( $f_q = 0.01$ ) activated instantaneously for different rates of pressure decline: (a)  $S_g$  vs  $t$ ; (b)  $S_g$  vs  $P_\infty$ .

fraction,  $f_q$ , where all sites are simultaneously activated at the onset of the processes [case (c)], is shown in Fig. 12. As anticipated, the saturation at a fixed time (or pressure) increases with  $f_q$ .

##### 5. CRITICAL GAS SATURATION

We are now in a position to determine the critical gas saturation,  $S_{gc}$ , which was introduced as the critical value of the gas-occupied pore volume fraction at which a sample-spanning gas cluster forms. To understand the effects of the various factors on  $S_{gc}$ , we must consider the various patterns discussed in Section 4.

##### 5.1. $S_{gc}$ at global percolation

At conditions of global percolation,  $S_{gc}$  is only dependent on the nucleation fraction, specifically on the interdependence between pore and cavity size distributions,  $\alpha(r)$  and  $F(W)$ , respectively, and on the system size,  $L$  (expressed as lattice size). When only one site is allowed for nucleation, the critical gas saturation coincides with the volumetric fraction of the percolation cluster, the scaling of which follows the power law (Stauffer, 1985)

$$S_{gc}(0, L) \sim L^{D_f - E} = L^{-\beta/\nu} \quad (59)$$

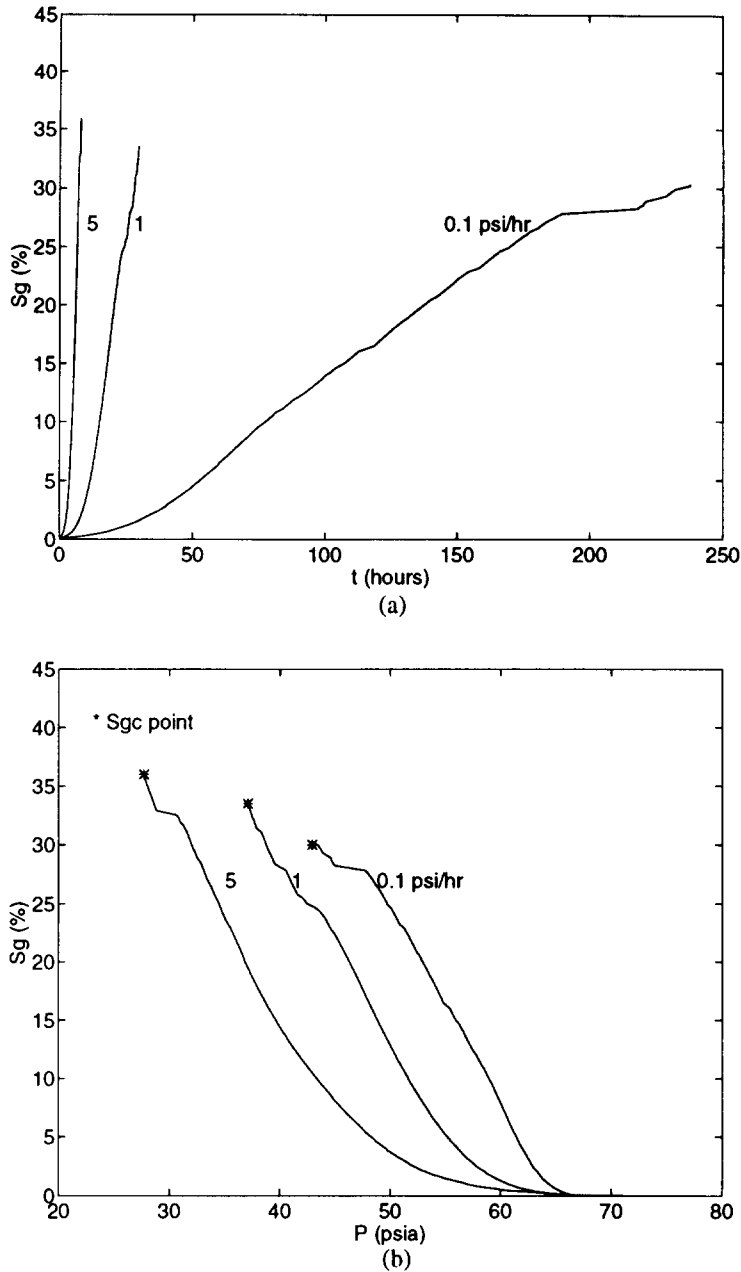


Fig. 11. Simulation of the evolution of gas saturation for sequential activation of 40 nucleation sites in a  $40 \times 40$  square lattice for different rates of pressure decline: (a)  $S_g$  vs  $t$ ; (b)  $S_g$  vs  $P_\infty$ .

where  $E$  denotes the Euclidean dimension of the porous medium, and  $\beta$  is the exponent scaling the percolation cluster mass [ $\beta \sim 0.14$  in 2-D and  $\beta \sim 0.43$  in 3-D, Stauffer (1985)]. It follows that  $S_{gc}(0)$  vanishes for a sufficiently large size  $L$ , although the asymptotic approach is quite slow ( $\sim L^{-0.11}$  in 2-D and  $\sim L^{-0.50}$  in 3-D). The slow decay in 2-D explains the large  $S_{gc}$  values typically obtained in 2-D micromodel experiments and in 2-D pore network simulations. It must be remembered that eq. (59) is valid as long as the size does not exceed the percolation boundary, beyond which percolation rules weaken.

When a non-zero nucleation fraction is involved, two cases need to be considered, one involving an

instantaneous, and another a sequential activation. In either case,  $S_{gc}$  consists of contributions from clusters growing from different nucleation centers until a sample-spanning cluster has formed. We may separate the contribution from the percolation cluster [the fractal contribution corresponding to eq. (59) above] from the contribution from the rest of the clusters (the Euclidean contribution). The latter is the sum of a number  $f_q L^E$  of nucleation centers, each contributing a total of  $(l/r^*)^{D_f}$  pores, thus

$$S_{gc}(f_q, L) = S_{gc}(0, L) + (\text{const}) \frac{f_q L^E (l/r^*)^{D_f}}{L^E}. \quad (60)$$

With the further approximation  $l \sim l_q$  and using a ver-

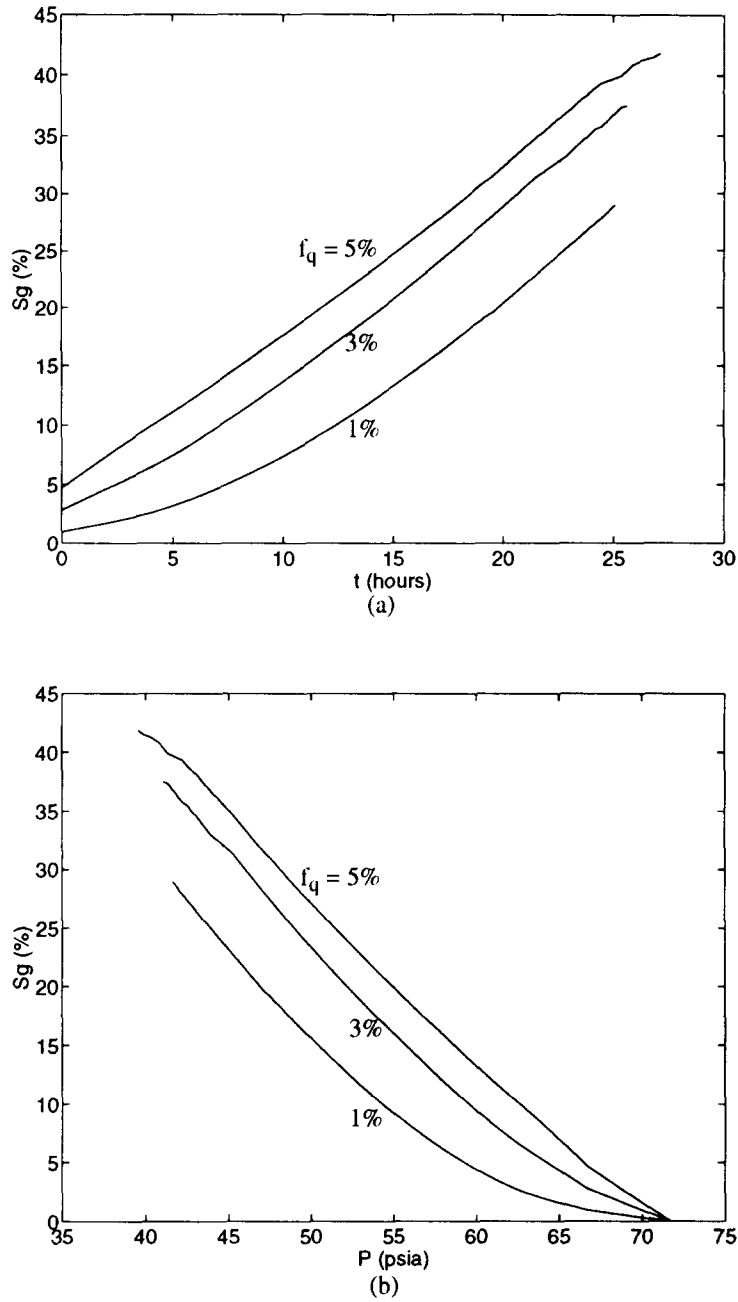


Fig. 12. Simulation of the effect of the nucleation fraction,  $f_q$ , on the gas saturation evolution for  $a = 1$  psi/h: (a)  $S_g$  vs  $t$ ; (b)  $S_g$  vs  $P_\infty$ .

sion of expression (39) with a generalized Euclidean dimension  $E$ , we obtain

$$S_{gc}(f_q, L) \sim (\text{const})L^{-\beta/\nu} + (\text{const})f_q^{\beta/\nu E}. \quad (61)$$

This approximation, valid at sufficiently small  $f_q$ , shows that the size scaling of the critical gas saturation is independent of the nucleation fraction. Nonetheless, the importance of size decreases as the nucleation fraction increases and, furthermore, for a sufficiently large size,  $S_{gc}$  is very sensitive to the nucleation fraction (e.g.  $S_{gc} \sim f_q^{0.05}$  in 2-D and  $S_{gc} \sim f_q^{0.16}$  in 3-D). This means that even *small* nucleation fractions have

a disproportionately *large* effect on  $S_{gc}$ . Typical plots of  $S_{gc}$  vs  $f_q$  from simulations in finite-size lattices are shown in Fig. 13. Consistent with the theory, the curves show a rapid increase of  $S_{gc}$  at low  $f_q$ , and a much slower growth at larger values.

In the case of sequential activation of sites,  $S_{gc}$  can in principle be determined given the pore and throat size distributions  $\alpha_s(r)$ ,  $\alpha_b(r)$ , and the nucleation site size distribution,  $F(W)$ . This approach was outlined by Yortsos and Parlar (1989) for a general problem and numerically illustrated for idealized *Bethe* lattices. A statistical analogue is to consider cluster growth

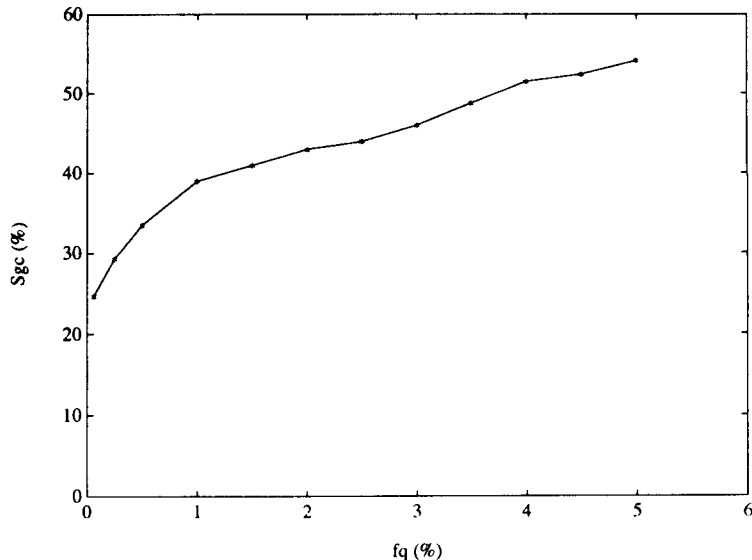


Fig. 13. Critical gas saturation vs nucleation fraction for global percolation regime.

from one site first, follow invasion percolation rules, and activate at random a new site  $i$  every  $M_i$  time steps (or occupied sites). For example, if the first nucleation cavity has size  $W_1$  (corresponding to the globally maximum cavity size), the fraction of eligible to be penetrated throats is  $p_1 = \int_{W_1}^{\infty} \alpha_b(r) dr$ , the fraction of the actually penetrated throats scales as  $P(p_1) \approx |p_1 - p_c|^a$ , and one may take  $M_1 = L^E P(p_1)$ . After the throats become penetrated, another pore is activated and growth from both clusters is possible. From now on the ratio of the newly activated pores to the pores *allowed* for penetration is equal to  $F(r_i)/\alpha_b(r_i)$ , although its ratio to the actually *invaded* pores,  $1/M_i$ , is larger because of the lack of accessibility,

$$\frac{1}{M_i} = \frac{F(r_i)}{\alpha_b(r_i)} \left( \frac{dp}{dP} \right). \quad (62)$$

Here,  $P$  is the invaded fraction of pores, clearly a function of the history of the process and of the bond percolation probability  $p$ . While the previous power-law scaling applies in the single cluster case, the general problem does not admit a universal power law, however, and must be solved separately for each case.

### 5.2. $S_{gc}$ at local percolation

While analytical results are possible for global percolation, the more general patterns discussed previously require a numerical solution. We consider the case of pressure decline rates sufficiently low for local percolation to apply, but sufficiently high for global percolation not to be enforced. As in the previous case, different results are obtained depending on the mode of nucleation.

When the pressure decline rate is fixed and all nucleation sites are activated at the onset of the process, an increase in nucleation fraction will generally result in an increase of  $S_{gc}$ . Shown in Fig. 14 are

simulation results for a  $40 \times 40$  network and a pressure decline rate of 1 psi/h. If no additional nucleation is allowed, the pressure decline rate does not affect significantly the critical gas saturation. This interesting and important result can be directly explained by reference to the two patterns described by eqs (43)–(45) and eqs (47)–(53), both of which assume weak supersaturation, such that convection is not very significant. Given the nucleation site positions, the succession of cluster growth obeys geometrical and topological rules which are independent of the pressure decline rate. Thus, although the time change of the pattern is a strong function of rate, its geometry is the *same* for all processes, *independently* of the decline rate. It follows that  $S_{gc}$ , which is a topological and geometric property, is also *independent* of  $a$  in this case. The numerical simulations in a  $40 \times 40$  lattice with 16 nucleation sites (Fig. 10) show that this is indeed the case over a wide range of pressure decline rates. The value of  $S_{gc}$ , however, does depend on the nucleation fraction as in the previous case of global percolation and we expect that  $S_{gc}$  has the same size scaling as  $S_{gc}(f_q, L)$  in eq. (60).

When nucleation occurs by successive site activation,  $S_{gc}$  is *dependent* on  $a$ , higher pressure decline rates resulting in higher critical gas saturations. The general interpretation of this effect is that at higher  $a$ , the effective supersaturation in the system is higher, as a result of both lower liquid pressure and slower depletion rates, thus giving rise to activation of ever smaller cavity sizes, thus to a larger nucleation fraction, and to a larger  $S_{gc}$ . This effect is clearly seen when model eqs (47)–(53) is used in the activation condition (1). We note that in the dimensionless notation, expression (1) becomes

$$C_{Dk} - \Pi_1 P_{Dk} \geq \frac{2\Pi_1}{Ca} \frac{1}{W_{Dk}} \quad (63)$$

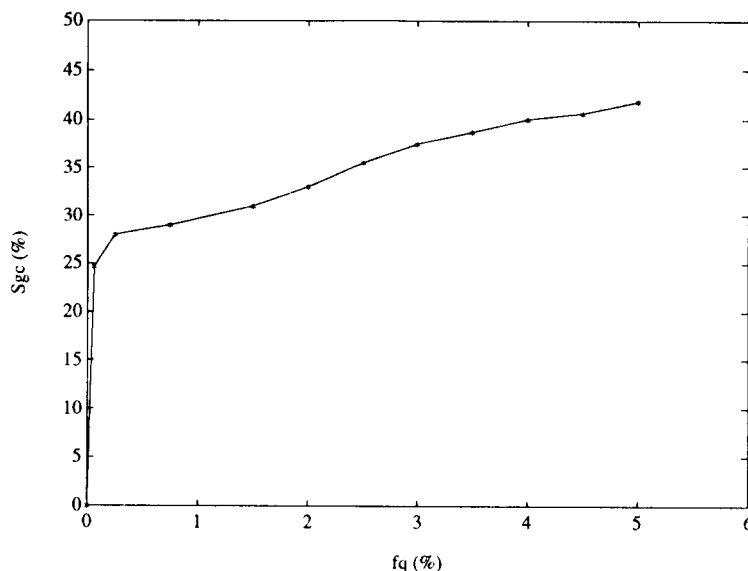


Fig. 14. Simulation of critical gas saturation vs nucleation fraction for  $a = 1$  psi/h.

where  $W$  was made dimensionless with the average pore size, and in view of  $\Pi_1 \ll 1$ , the condition reduces to one involving concentration only

$$C_{Dk} \geq \frac{2\Pi_1}{Ca} \frac{1}{W_{Dk}}. \quad (64)$$

In dimensional variables expression (64) implies that the supersaturation at any site is effectively given by the far-field pressure  $P_\infty$ . Consider, now the application of eq. (50) from the percolation-modified DLA pattern. After rearrangements inequality (64) becomes

$$W_{Dk} \geq \frac{2\gamma D}{ar^*l_q^2} \frac{1}{G(\mathbf{x}_k)}. \quad (65)$$

Because the precise value of  $G(\mathbf{x}_i)$  depends on the solution of the entire problem (47)–(53), it is certainly affected by the existence of various clusters. Given a configuration, however,  $G(\mathbf{x}_i)$  is fixed, independent of other process parameters. Then, relation (65) shows that there is a higher activation probability [lower right-hand side of relation (65)] at lower values of  $\gamma$ ,  $D$  and  $f_q$ , and at higher values of  $a$  and  $r^*$ . Thus, we anticipate that the nucleation fraction would increase with an increase in  $a$ , and that as more nucleation sites become activated, further nucleation becomes progressively more difficult and may possibly terminate. The numerical simulations of Fig. 11 confirm these trends.

Incidentally, we note that expression (65) in conjunction with some simple geometries for the solution of eqs (47)–(53) can be used to provide estimates on nucleation conditions. For example, if only one cluster, with center at the origin and effective radius  $R$ , is considered, and  $G(\mathbf{x})$  is approximated by the effective medium solution around this cluster,  $G = (1/6)(R^2 - |\mathbf{x}|^2) + (R_e/3)(|\mathbf{x}| - R)$ , where  $R_e$  is the outer boundary and spherical symmetry was as-

sumed, further nucleation will not occur if

$$W_{\max} < \frac{12\gamma D}{a(R_e - R)^2} \quad (66)$$

a condition likely to be satisfied at very low  $a$ , everything else being fixed, but to be progressively worse as time (and  $R$ ) increase.

## 6. CONCLUDING REMARKS

In this paper, a theoretical analysis of bubble growth processes in porous media, with particular emphasis on solution gas-drive, were developed. The model included nucleation, phase equilibria, mass transfer, capillary and viscous effects. Both single and multiple cluster growth were analyzed in terms of growth patterns and rates of growth

For a single cluster, the pattern is invasion percolation from a single source at sufficiently small sizes, low capillary numbers and supersaturations, but becomes a viscous fingering pattern at sufficiently large sizes. The rate of growth of a single cluster was found to scale differently than in the classical growth in the bulk, reflecting the porous media characteristics. For the multiple cluster problem, the existence of multiple nucleation centers affects the process dynamics. At sufficiently low pressure decline rates, a global percolation pattern develops, in which growth is completely controlled by capillarity. At higher decline rates, although each cluster follows percolation rules, the rates of cluster growth are dictated by mass transfer, which in some cases can be modeled by a DLA model. Appropriate patterns were identified.

The critical gas saturation value depends on the underlying growth pattern. At conditions of global percolation,  $S_{gc}$  only depends on the nucleation fraction, here assumed to be due to the existence of specific nucleation sites. Nucleation is significant for

the other patterns as well. When all nucleation sites are activated at once,  $S_{gc}$  is not affected by the pressure decline rate, but depends on the nucleation fraction only. On the other hand,  $S_{gc}$  depends on the pressure decline rate, generally increasing with  $a$ , when site activation is sequential. In the latter case, the critical gas saturation also increases with the nucleation fraction.

An important question of relevance to practical and field applications concerns the scale-up of the results derived. For the case of single cluster growth, the scaling theory of equations (27)–(37) is applicable. For the case of multiple cluster growth, the various sub-cases must be separately examined. If the pressure decline rate is sufficiently small such that expression (42) is obeyed, the gas saturation evolves according to eq. (58), which shows the dependence on  $a$  and  $P_0$ , with the critical gas saturation scaling according to eqs (59)–(61). Because the numerical simulations presented here correspond to a 2-D network, finite size effects are strong and result in  $S_{gc}$  values much larger than in an actual physical system. Also, because of the small sizes involved, the numerical values are sensitive to the particular realizations taken in activation sites, different realizations leading to different  $S_{gc}$  values. For realistic values, a much larger system in 3-D must be solved. This is currently under consideration. If a regime other than global percolation applies, strong finite size effects on  $S_{gc}$  are also expected. However, given a sufficiently large system in a 3-D lattice, these effects can be successfully eliminated. Early growth rates should be tractable by the single cluster problem described above, while late growth rates scale in an implicit fashion with the degree of supersaturation  $S$ , the growth rate group  $al_q^2/DP_0$ , and the nucleation activation condition (65). In the multiple cluster problem, the implicit assumption has been made that viscous forces are negligible over capillarity, which is satisfied if condition (40) holds. Because of the relatively low values of  $Ca$ , this is likely to be the case in all practical applications. Following the creation of a sample-spanning cluster, however, viscous effects should be tested as in typical gas–liquid displacements (Rege and Fogler, 1988).

An additional remark pertains to the physical processes following the onset of  $S_{gc}$ . In a finite system, such as a laboratory core, gas flow at the outlet end would commence following the onset of a sample-spanning cluster. The production of the gas is now the result of both diffusion and displacement of the gas phase out of the porous medium. Because of the pressure condition at the outlet, this type of displacement resembles counter-current imbibition and may lead to the break-up of the sample-spanning cluster. The result would be a lowering of the gas saturation in the system, and the subsequent growth of other gas clusters. In a large-scale system, the practice is usually taken to assign  $S_{gc}$  as the end-point value to curve-fit a secondary drainage relative permeability curve. This is not correct, strictly speaking. The development of gas saturation has become possible through nuclea-

tion events, rather than external invasion, and the corresponding flow function ought to reflect this. Analytical results for relative permeabilities in Bethe lattices were derived by Yortsos and Parlar (1989) with the nucleation fraction included as a parameter. However, related results in regular 3-D lattices do not exist at present.

Although a comprehensive analysis of the effect of gravity was not attempted, it is rather straightforward to delineate the conditions under which it can be neglected. In the case of a single cluster, the percolation boundary is simply obtained from a balance of gravity and capillary forces which yields a condition similar to Section 2, where the Bond number,  $B_g = \Delta\rho g(r^*)^2/\gamma$ , is substituted in place of the capillary number. Gravity effects on the interface concentration would be unimportant as long as the relative variation is negligible, namely when the following conditions are satisfied:

$$\frac{\rho_l g r^*}{P_0} \left( \frac{R}{r^*} \right) \ll 1 \quad (67)$$

and

$$\frac{\rho_l g r^*}{P_0} \ll (\phi f_q)^{1/3} \quad (68)$$

for the case of a single cluster of size  $R$ , and for a multiple cluster problem, respectively. We anticipate important effects of gravity when either of these is violated, the likelihood of which increases in high permeability and low pressure systems.

*Acknowledgements*—This work was partly supported by a grant from Chevron Oil Field Research (now Chevron Petroleum Technology Corporation). Additional support was provided by the USC Center for the Study of Fractured Reservoirs, supported by Aramco, Mineral Management Services, State Lands Commission of California, Texaco E & P and Unocal Science & Technology. All these sources of support are gratefully acknowledged. Useful discussions with Jairam Kamath are also acknowledged.

#### NOTATION

$a$	pressure decline rate, Pa/s
$A$	surface area, m <sup>2</sup>
$C$	concentration of solute (dissolved gas), kg/m <sup>3</sup>
$Ca$	capillary number (dimensionless)
$Ca'$	modified capillary number (dimensionless)
$C_0$	initial concentration of solute, kg/m <sup>3</sup>
$C_\infty$	far-field concentration of solute, kg/m <sup>3</sup>
$D$	diffusion coefficient, m <sup>2</sup> /s
$D_f$	fractal dimension
$E$	Euclidean dimension
$f_q$	nucleation fraction
$F$	cavity size distribution, m <sup>-1</sup>
$Ja$	Jakob number (dimensionless)
$k$	permeability, m <sup>2</sup>
$K$	solubility constant, Pa/(kg/m <sup>3</sup> )
$l$	length, m
$L$	lattice extent, m
$M$	random walker number
$M_w$	molecular weight, kg/mol

$n$	number of moles, mol
$N$	number of pores in a cluster
$P$	pressure, Pa
$P_0$	initial system pressure, Pa
$P_\infty$	far-field system pressure, Pa
$P_c$	capillary pressure, Pa
$Q$	liquid withdrawal rate, m <sup>3</sup> /s
$r$	pore radius, m
$R$	radius of gyration, m
$R_e$	outer boundary radius, m
$\mathcal{R}$	ideal gas constant, J/mol/K
$S$	supersaturation (dimensionless)
$S_g$	gas saturation (dimensionless)
$S_{gc}$	critical gas saturation (dimensionless)
$t$	time, s
$T$	temperature, K
$u$	velocity, m/s
$V$	volume, m <sup>3</sup>
$W$	cavity radius, m

**Greek letters**

$\alpha$	dimensionless solubility constant
$\beta$	percolation probability exponent
$\gamma$	interfacial tension, N/m
$\lambda$	dimensionless pressure drop for case (ii)
$\mu$	viscosity, Pa s
$\nu$	correlation length exponent
$\rho$	density, kg/m <sup>3</sup>
$\sigma$	standard deviation
$\tau$	dimensionless time
$\phi$	porosity (dimensionless)

**Superscripts**

*	characteristic value
$p$	percolation
$vf$	viscous fingering

**Subscripts**

$D$	dimensionless
$f$	filling stage
$g$	gas
$i$	pore $i$
$j$	pore $j$
$k$	cluster $k$
$l$	liquid
$m$	pore $m$
$p$	pressurizing stage
$T$	total

**REFERENCES**

- Atchley, A. A. and Prosperetti, A., 1989, The crevice model of bubble nucleation. *J. Acoust. Soc. Am.* **86** (3), 1065–1084.
- Blunt, M. and King, P., 1991, Relative permeabilities from two- and three-dimensional pore-scale network modeling. *Transport Porous Media* **6**, 407–433.
- Chatenever, A., Indra, M. K. and Kyte, J. R., 1959, Microscopic observation of solution gas-drive behavior. *Journal of Petroleum Technology* **11**, 13–15.
- Chowdiah, P., 1987, Laboratory measurements relevant to two-phase flow in a tight gas sand matrix. SPE 16945, presented at the 62nd Annual Technical and Exhibition of the SPE in Dallas, TX, 27–30 September.
- Crum, L. A., 1982, Nucleation and stabilization of micro-bubbles in liquids. *Appl. Sci. Res.* **38**, 101–115.
- Danesh, A., Peden, J. M., Krinis, D. and Henderson, G. D., 1987, Pore level visual investigation of oil recovery by solution gas drive and gas injection. SPE 16956, presented at the 62nd Annual Technical and Exhibition of the SPE in Dallas, TX, 27–30 September.
- Doughty, C. and Pruess, K., 1988, A semianalytical solution for heat-pipe effects near high-level nuclear waste package buried in partially saturated geological media. *Int. J. Heat Mass Transfer* **31**, 79–90.
- Dullien, F.A.L., 1992, *Porous Media, Fluid Transport and Pore Structure*, 2nd Edition, Academic Press, San Diego.
- Dumoré, J. M., 1970, Development of gas saturation during solution gas drive in an oil layer below a gas cap. *SPEJ*, 211–218.
- Firoozabadi, A., Ottesen, B. and Mikklesen, M., 1989, Measurement and modeling of supersaturation and critical gas saturation: part 1, measurements. SPE 19694, presented at the 64th Annual Technical and Exhibition of the SPE in San Antonio, TX, 8–11 October.
- Handy, L. L., 1958, A laboratory study of oil recovery by solution gas drive. *AIME Trans.* **213**, 310–315.
- Hoyos, M., Moulou, J. C., Deflandre, F. and Lenormand, R., 1990, Ultrasonic measurements of the bubble nucleation rate during depletion experiments in a rock sample. SPE 20525, presented at the 65th Annual Technical and Exhibition of the SPE in New Orleans, LA, 23–26 September.
- Hunt, E. B. Jr., and Berry, V. J. Jr., 1956, Evolution of gas from liquids flowing through porous media. *A.I.Ch.E. J.* **2**, 560–567.
- Kamath, J. and Boyer, R. E., 1993, Critical gas saturation and supersaturation in low permeability rocks. Paper SPE 26663, presented at the 68th Annual Technical Conference and Exhibition of the SPE, Houston, TX, 3–6 October.
- Kashchiev, D. and Firoozabadi, A., 1993a, Kinetics of the initial stage of isothermal gas phase formation. *J. Chem. Phys.* **98** (6), 1.
- Kashchiev, D. and Firoozabadi, A., 1993b, Pressure and volume evolution during gas phase formation in solution gas drive process. SPE 26286.
- Kennedy, H. T. and Olson, C. R., 1952, Bubble formation in supersaturated hydrocarbon mixtures. *AIME Trans.* **195**, 271–278.
- Knight, R., Chapman, A. and Knoll, M., 1990, Numerical modelling of microscopic fluid distribution in porous media. *J. Appl. Phys.* **68**, 994–1001.
- Kortekaas, T. F. M. and Poelgeest, F. V., 1989, Liberation of solution gas during pressure depletion of virgin and watered-out reservoirs. SPE 19693, presented at the 64th Annual Technical and Exhibition of the SPE in San Antonio, TX, 8–11 October.
- Lenormand, R., Touboul, E. and Zarcone, C., 1988, Numerical models and experiments on the immiscible displacements in porous media. *J. Fluid Mech.* **189**, 165–187.
- Lenormand, R., 1989, Flow in porous media: limits of fractal patterns. *Proc. Roy. Soc.* **A423**, 159–168.
- Lenormand, R., 1990, Liquids in porous media. *J. Phys.: Condens. Matter* **2**, SA79–SA88.
- Li, X. and Yortsos, Y. C., 1991, Visualization and numerical studies of bubble growth during pressure depletion. SPE 22589, presented at the 66th Annual Technical and Exhibition of the SPE, Dallas, TX, 6–9 October (revised version, *A.I.Ch.E. J.*, in press).
- Li, X. and Yortsos, Y. C., 1994, Bubble growth and stability in an effective porous medium. *Phys. Fluids A* **6** (5), 1663–1676.
- Moulou, J. C. and Longeron, D., 1989, Solution-gas drive: experiments and simulation. Paper presented at the 5th European Symposium on Improved Oil Recovery, Budapest, Hungary.
- Platt, C. R. and Lewis, W. M., 1969, Analysis of unusual performance indicates high solution-gas-drive recovery-stalene ellenburger field. *Journal of Petroleum Technology*, **21**, 1507–1509.

- Plesset, M. S. and Prosperetti, A., 1977, Bubble dynamics and cavitation. *Ann. Rev. Fluid Mech.* **9** 145–185.
- Rege, S. D. and Fogler, H. S., 1988, A network model for deep bed filtration of solid particles and emulsion drops. *A.I.Ch.E. J.* **34**, 1761–1772.
- Satik, C., Li, X. and Yortsos, Y. C., 1995, Scaling of bubble growth in a porous medium. *Phys. Rev. E*, in press.
- Schubert, G. and Straus, J. M., 1977, Two-phase convection in a porous medium. *J. Geophys. Res.* **82**, 3411–3421.
- Scriven, L. E., 1959, On the dynamics of phase growth. *Chem. Engng Sci.* **10** 1–13.
- Stauffer, D., 1985, *Introduction to Percolation Theory*. Taylor and Francis, London.
- Stewart, C. R., Craig, F. F. and Morse, R. A., 1953, Determination of limestone performance characteristics by model flow tests. *AMIE Trans.* **198**, 93–102.
- Szekely, J. and Martins, G. P., 1971, Non-equilibrium effects in the growth of spherical gas bubbles due to solute diffusion. *Chem Engng Sci.* **26**, 147–159.
- Szekely, J. and Fang, S. D., 1973, Non-equilibrium effects in the growth of spherical gas bubbles due to solute diffusion—II: the combined effects of viscosity, liquid inertia, surface tension and surface kinetics. *Chem. Engng Sci.* **28**, 2127–2140.
- Thome, J. R., 1990, *Enhanced Boiling Heat Transfer*, Hemisphere, Washington.
- Wieland, D. R. and Kennedy, H. T., 1957, Measurement of bubble frequency in cores. *AIME Trans.* **210**, 123–125.
- Yortsos, Y. C. and Parlar, M., 1989, Phase change in binary systems in porous media: application to solution gas drive. SPE 19697, presented at the 64th Annual Technical and Exhibition of the SPE in San Antonio, TX, 8–11 October.
- Yousfi, El., Zarcone, C., Bories, S. and Lenormand, R., 1990, Poster Paper Presented at the 5th IFP Research Conference, Arles, France 14–18 May.
- Yousfi, El., Zarcone, C., Bories, S. and Lenormand, R., 1991, Mechanisms of solution gas liberation during pressure depletion in porous media. *C. R. Acad. Sci. Paris t. 313*, Serie II, 1093–1098.

#### APPENDIX A

The following remarks are appropriate regarding the two steps of pressurization and pore filling taken to represent bubble growth.

**Remark 1:** Across any meniscus, the proper interface conditions are

$$u_n = V_n \quad (\text{A1})$$

$$\rho_g(V_n - u_{gn}) = D \frac{\partial C}{\partial n} \quad (\text{A2})$$

where  $u_{gn}$  is the normal component of the gas velocity at the interface and  $V_n$  the normal interface velocity. Diffusion to a stationary interface ( $V_n = 0$ ) results in a net gas flux into the cluster away from the interface ( $u_{gn} < 0$ ), which subsequently affects through eq. (A2) the rate of growth of other advancing interfaces ( $V_n \neq 0$ ). To determine  $u_{gn}$  requires the solution of the gas momentum equation. Without loss in generality, we elected not to do so, and to solve for the integral balances (9) and (10) only. Consideration of transport in a growing phase of a non-negligible viscosity, however, is important in stability problems (Li and Yortsos, 1994).

**Remark 2:** It is useful to provide an estimate of the relative time increments involved in the two steps. The ratio of the time pressurization,  $\Delta t_{pk}$ , to the time of filling,  $\Delta t_{fk}$ , of cluster  $k$  is roughly equal to

$$\frac{\Delta t_{pk}}{\Delta t_{fk}} \sim \frac{V_k P_c}{V_s P_i} \quad (\text{A3})$$

where  $P_c$  measures a typical capillary pressure, and  $V_s$  de-

notes the volume of a single pore. Because we can further take the approximation  $V \approx N_k V_s$ , where  $N_k$  denotes the number of sites in cluster  $k$ , expression (A3) suggests that for small clusters and low capillary pressure (high permeability) systems the pressurization step is much faster than the filling step, while for large clusters and high capillary pressures (low permeabilities) it becomes comparable to or slower than the filling step.

**Remark 3:** During the filling step, we assume that the capillary pressure is negligible and that only the newly invaded pore is filled. In reality, when the threshold is reached and the invasion of a new pore begins (which constitutes a "rheon" event) all other menisci in the bubble interface recede somewhat, the corresponding pores becoming slightly less occupied. This small loss of volume is replaced during the subsequent filling step. Such a sequence has been actually observed in our experiments for small size clusters. Simulation results showed very small differences when the more detailed mechanism was included, thus we proceeded to neglect it.

**Remark 4:** Immediately following penetration of the throat, and due to the relaxation of the capillary pressure requirements, rapid volume expansion takes place, during which mass transfer is negligible. The corresponding volume expansion during this step,  $\Delta V_e$ , is

$$\frac{\Delta V_e}{V_s} = N_k \frac{P_c}{P_i} \quad (\text{A4})$$

For small cluster sizes or low capillary pressure systems,  $\Delta V_e$  is smaller than the site volume hence the previous approach can be used. On the other hand, if  $\Delta V_e > V_s$ , the possible penetration of additional pore throats may occur within a very short time and in the absence of significant mass transfer. Appropriate modifications are then necessary.

#### APPENDIX B

An important question in relation to Section 3 is the validity of the quasi-static approximation. For compact patterns (bulk growth) under the conditions of case (i), the appropriate condition is readily shown to be  $Ja \ll 1$ , uniformly in time. However, this is not necessarily true for the case of fractal patterns in either case (i) or (iii). Consider the solution of eq. (21) in the limit  $S \ll 1$

$$C_D = -\frac{R_D}{r} + 1 \quad (\text{B1})$$

where  $R$  is related to  $\tau$  through eq. (32). This approximation is well satisfied if the condition  $S|\partial C_D/\partial \tau| \ll |\partial^2 C_D/\partial r^2|$  applies at  $r = R$ , which, in view of eq. (B1), is

$$S\tau^{(3-D_f)/(D_f-1)} \ll 1. \quad (\text{B2})$$

In fractal patterns ( $D_f < 3$ ), and contrary to the compact cluster case ( $D_f = 3$ ), the validity of the approximation is time-dependent. To determine whether eq. (B2) is still applicable when the percolation boundary is encountered, we solve eq. (32) for  $\tau$ , make use of eq. (27), and substitute the results in eq. (B2) to obtain the following condition at the percolation boundary:

$$S^{1-(v/(v+1))(3-D_f)} \ll 1. \quad (\text{B3})$$

For the typical values  $v = 0.88$  and  $D_f = 2.5$ , the above is equivalent to  $S \ll 1$ . For case (i), the latter translates into the condition  $Ja \ll 1$ , uniformly in time, as in the bulk. For case (iii), however, some additional work is necessary. Here the growth of a single bubble can be graphically traced (by eliminating time) by a straight line in a  $R$  vs  $Ca$  log-log plot. By rearranging eq. (32) we rewrite

$$\left(\frac{R}{r^*}\right)^{D_f-1} = \frac{4\pi\alpha(D_f-1)}{D_f} \left(\frac{DP_0}{ar^{*2}}\right) \frac{Ca^2}{(D\mu r^*/\gamma k)}. \quad (\text{B4})$$

The intersection of  $R$  with the percolation boundary,  $R^p$ , gives the critical time  $t_p$  at which the transition from percolation to viscous fingering commences. We can readily show that the corresponding supersaturation  $S_p$  satisfies the scaling

$$S_p \sim \left( \frac{ar^{*2}}{DP_0} \right)^{[(v+1)/(v(1+D_f)+2)]} \left( \frac{D\mu r^*}{\gamma k} \right)^{-1/(D_f-1)/(v(1+D_f)+2)} \quad (\text{B5})$$

For the quasi-static assumption to remain valid until this boundary is reached, requires  $S_p \ll 1$ , which for typical conditions ( $a \sim 1$  psi/day,  $P_0 \sim 1000$  psi,  $D \sim 10^{-5}$  cm<sup>2</sup>/s,  $\mu \sim 1$  cp,  $r^* \sim 1$   $\mu$ m and  $\gamma \sim 60$  dyn/cm) is easily satisfied.

We conclude that the previously derived scalings are valid provided that  $Ja \ll 1$  for case (i) and  $S_p \ll 1$  for the case (iii). It is interesting to inquire about the concentration fields for case (ii). Quasi-static mass transfer implies a supersaturation  $S$  varying as

$$S \sim \frac{Q}{4\pi\alpha Dr^* R_D} \quad (\text{B6})$$

Since the latter decreases with an increase in cluster size, the quasi-static assumption ( $S \ll 1$ ) should be questionable at least in the early times of the process. In fact, however, it is doubtful whether quasi-static conditions apply at all during the percolation regime, because this would require

$$\left( \frac{Q\mu}{\gamma r^{*2}} \right)^{1/v} \left( \frac{Q}{Dr} \right) \ll 4\pi\alpha \quad (\text{B7})$$

as shown by substituting expression (B6) into expression (30), which is unlikely to be satisfied under typical conditions. Of course, this does not affect the validity of the percolation boundary or the scaling eq. (35), both of which were derived independently of mass transfer considerations.

Similar considerations apply for the viscous fingering boundary. For case (i), the analogous to expression (42) equation reads

$$S^{1-[D_f(3-D_f)/(D_f-1)]} \ll 1 \quad (\text{B8})$$

which is equivalent to the bulk condition  $Ja \ll 1$ , since  $D_f \sim 2.5$  for 3- $D$  viscous fingering. For case (iii) of variable  $a$ , the intersection of the curve of the radius  $R$  with the viscous fingering boundary  $R_{vf}$  yields the supersaturation  $S_{vf}$ , which can be approximated by

$$S_{vf} \sim \left( \frac{ar^{*2}}{DP_0} \right)^{1/(D_f+1)} \left( \frac{D\mu r^*}{k\gamma} \right)^{-D_f/(D_f+1)} \quad (\text{B9})$$

The quasi-static approximation requires  $S_{vf} \ll 1$ , which is expected to be valid at sufficiently small values of  $a$ .

#### APPENDIX C

It was shown in Section 4, that for global percolation to be applicable the following condition must hold:

$$C_\infty(t) - P_0 + at \leq \frac{2\gamma}{Kr_p} \quad (\text{C1})$$

which states that the effective supersaturation in the system

remains bounded and it is of the same order of magnitude as the capillary pressure level. To derive a condition on  $a$  from inequality (C1), we need an estimate of  $C_\infty(t)$ . Under the assumption of small concentration gradients, we obtain from mass balances

$$\frac{dC_\infty}{dt}(1 - S_g) = -\frac{1}{V_T} D \int_{A_T} \frac{\partial C}{\partial n} dA \quad (\text{C2})$$

where  $S_g$  is the gas saturation,  $V_T$  refers to the total pore volume and  $A_T$  is the total area for mass transfer. The mass transfer term in eq. (C2) must be evaluated over all clusters, clearly a difficult task. However, we can obtain a rough estimate by using the quasi-static approximation and assuming that the mass transfer to all other clusters is a small fraction  $\varepsilon$  of the rate to the growing cluster (recall that only one cluster grows at-a-time in this regime). Then, we obtain

$$\frac{dC_\infty}{dt}(1 - S_g) = -4\pi DR(t)(C_\infty - C_i) \times \left( \frac{1}{V_T} + \frac{\varepsilon\phi}{r^{*3}f_q} \right) \quad (\text{C3})$$

where  $R$  is the radius of the growing cluster. The growth of the latter can be expressed as

$$(r^*)^3 P_0 \frac{d}{dt} \left( \frac{R}{r^*} \right)^{D_f} = -\frac{R_g T}{M_w} \times \frac{(1 - S_g)}{\left[ \frac{1}{V_T} + \frac{\varepsilon\phi}{(r^*)^3 f_q} \right]} \frac{dC_\infty}{dt} \quad (\text{C4})$$

where, in view of eq. (31),

$$\frac{dS_g}{dt} = \frac{r^*}{V_T} \frac{d}{dt} \left( \frac{R_g}{r^*} \right)^{D_f} \quad (\text{C5})$$

These three equations can be reduced to one equation relating the variation of  $C_\infty$  to  $C_i \equiv (P_0 - at)/K$ . Assuming sufficiently small  $S_g$ , one finds the approximate equation

$$\frac{dC_\infty}{dC_i} \simeq \left[ \frac{4\pi DP_0}{(r^*)^2 a} \left( \frac{\varepsilon\phi f_q}{1 - S_g} \right)^{1-1/D_f} \alpha^{1/D_f} \right] \times \left( 1 - \frac{C_\infty}{C_0} \right)^{1/D_f} \left( \frac{C_\infty - C_i}{C_0} \right) \quad (\text{C6})$$

to be solved subject to the initial condition  $C_\infty = C_0$ ,  $C_i = C_0 - 2\gamma/Kr_1$ , where  $2\gamma/r_1$  is the initial supersaturation at the onset of growth. The condition for global percolation is that  $C_\infty$  stays close to  $C_i$  to within the capillary pressure limit. Because an asymptotic solution to expression (C6) is  $C_\infty \sim C_i + \Sigma$  where

$$\Sigma \sim \frac{a(r^*)^2 C_0}{DP_0(\varepsilon\phi f_q)^{1-1/D_f} \alpha^{1/D_f}} \quad (\text{C7})$$

a reasonably good estimate of the condition for global percolation is  $\Sigma < 2\gamma/Kr^*$ , which translates into eq. (42) in the text.